

53. SUMMARY LITHOLOGY AND SHIPBOARD X-RAY MINERALOGY OF BRAZIL BASIN AND RIO GRANDE RISE, DEEP SEA DRILLING PROJECT SITES 515 TO 518¹

William T. Coulbourn, Scripps Institution of Oceanography, La Jolla, California

ABSTRACT

Sites 515 to 518 were continuously cored during Leg 72. Sediment mineralogy determined from visual examination of core sections, microscopic inspection of smear slides, and interpretation of X-ray diffractograms made from 436 bulk samples from those sites reveal aspects of the Coniacian to Recent regional history of sedimentation in the Brazil Basin and on the Rio Grande Rise.

Drilling in the Brazil Basin at Site 515 penetrated Recent to Oligocene terrigenous and biogenic siliceous muds, and limy Eocene muds. Quartz occurs throughout; illite is dominant in the Quaternary and Pliocene and montmorillonite in the Miocene and Oligocene muds. Kaolinite is common in the Quaternary and Pliocene sediments, the whole of which are punctuated by carbonate-rich laminations and beds. Phillipsite is common in the Oligocene to Recent sediments, and clinoptilolite dominates the Eocene calcitic muds. A pronounced lag deposit in 515B-55,CC marks an unconformity that separates multicolored, extensively bioturbated lower Eocene sediments from overlying upper Oligocene siliceous mudstones.

The lithologic section at Site 516 on the Rio Grande Rise is dominantly carbonate with a succession of dominant clay components: illite in the Recent to Oligocene pelagic carbonate ooze and chalk; montmorillonite in the Eocene volcanogenic limestone; illite again in the Paleocene to lower Maestrichtian flaser limestone; kaolinite in the Campanian and Santonian limestone and marly limestone; montmorillonite again in the Coniacian *Inoceramus*-bearing limestone. Important diagenetic events are the chertification of the Eocene deposits and dolomitization of the Paleocene and Cretaceous deep-water limestones.

The shallow penetration hydraulic piston cores from Sites 517 and 518, located on the western flank of the Rio Grande Rise, are dominantly carbonates. An illite-rich bed in the middle Miocene sediments of Site 518 records a time of intense dissolution, perhaps an episode of abundant northward flow of Antarctic Bottom Water.

INTRODUCTION

This summary of the lithology of cores from Deep Sea Drilling Project Sites 515 to 518 relies on visual and smear slide observations, and on X-ray diffraction analysis of samples collected during the Leg 72 voyage of the *Glomar Challenger*. It is likely to be the first of a series, following the installation of a Rigaku table-top diffractometer on board *Glomar Challenger*. Although other reports, particularly Volume 39 of the DSDP *Initial Reports* (Supko, Perch-Nielsen, et al., 1977), McCoy and others (1977), and Zimmerman (1977), consider the lithology and clay mineral stratigraphy of southwestern Atlantic DSDP sites, this one is the first in which a large number of samples were analyzed as the cores were being described. This "on-line" analysis improves the chances of sampling intervals representative of both background and unusual lithologies, and provides a means of verification of shipboard visual determinations. Coupled with continuous coring during Leg 72, this type of analysis makes possible the documentation of source area and diagenetic effects for these sites. Although the analyses may be less precise than those from shore-based instruments, the availability of a diffractometer on board ship during a 2-month, 24-hr./day scientific endeavor has the potential of generating a great number of analyses. This chapter focuses on the interpretation of 436 X-ray diffractograms (XRDs) from bulk

samples, and compares those results with the visual core descriptions, physical properties, and seismic stratigraphy discussed in other contributions to this volume. The focus of the three companion mineralogic reports in this volume is somewhat different; Zimmerman discusses X-ray diffraction analysis of acid-treated samples. Emelyanov and Trimonis present the results of both geochemical and X-ray diffraction analyses of selected samples, and Levitan and others discuss cherts from Hole 516F.

The primary objectives of Leg 72 were to investigate the history of water mass distribution and movement in the ever-widening South Atlantic, as that history is recorded in the sediments of the seafloor (Barker et al., 1981; Johnson, this volume). The Leg 72 sites are arranged in a depth transect between the Brazil Basin and the Rio Grande Rise and range from 4252 m in the Brazil Basin to 3944 to 1313 m along the eastern flank of the Vema Channel (Fig. 1). This channel is the lowest passage through the east-west trending barrier formed by the Rio Grande Rise (LePichon et al., 1971). The Leg 72 sites complement others drilled during DSDP Legs 3 and 39 (Table 1). Site 515 is located in the Brazil Basin, well to the southwest of Site 355 and to the northeast of Site 356; and Site 516 is situated on the Rio Grande Rise near Sites 22 and 357. Site 515 is located far enough from the Vema Channel that the onset of vigorous thermohaline circulation in the latest Eocene, particularly the northward flow of Antarctic Bottom Water (AABW) might not have been recorded as a major unconformity (Site 515 chapter, this volume). Incidentally, Biscaye (1965)

¹ Barker, P. F., Carlson, R. L., Johnson, D. A., et al., *Init. Repts. DSDP, 72*: Washington (U.S. Govt. Printing Office).

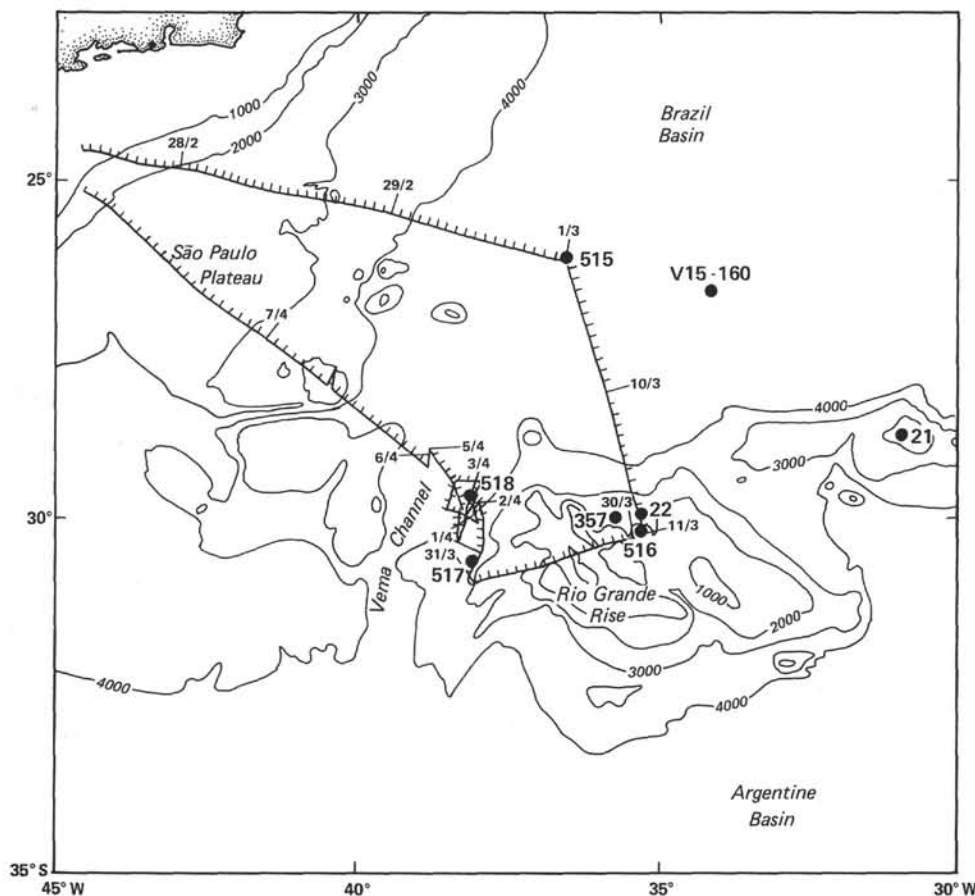


Figure 1. *Glomar Challenger* track line plot and location of DSDP sites in the southwestern Atlantic Ocean (after Barker et al., 1981). V15-160 designates the position of a piston core described in Zimmerman (1977). Contour interval is 1000 m. Day/month are listed along trackline.

Table 1. Coring summary for Rio Grande Rise and southwestern Atlantic Ocean DSDP sites drilled during Legs 3, 39, and 72.

Hole	Latitude ^a	Longitude ^b	Water depth (m)	Penetration (m)	Number of cores	Meters cored	Meters recovered
Leg 3							
21	28°35.10'	30°35.85'	2113	131.0	9	101	72.5
21A	28°35.10'	30°35.85'	2113	79.3	3		26.8
22	30°00.31'	35°15.00'	2134	242.0	5		44.5
Leg 39							
355	15°42.59'	30°36.03'	4886	460.0	22	207.5	118.1
356	28°17.22'	41°05.28'	3175	741.0	44	418.0	215.9
356A	28°17.22'	41°05.28'	3175	38	2	19	17.6
357	30°00.25'	35°33.59'	2086	796.5	51	473.0	345.2
Leg 72							
515	26°14.33'	36°30.17'	4250	55.5	3	17.5	5.5
515A	26°14.31'	36°30.17'	4252	107.9	27	107.9	95.7
515B	26°14.32'	36°30.19'	4252	636.4	57	541.5	429.1
516	30°16.58'	35°17.11'	1313	183.3	44	183.3	148.1
516A	30°16.59'	35°17.12'	1313	69.5	16	69.5	61.1
516B	30°16.59'	35°17.12'	1317	23.2	1	7.6	4.5
516C	30°16.59'	35°17.12'	1313	20.6	1	6.5	0.0
516D	30°16.56'	35°17.11'	1313	90.1	0	0.0	0.0
516E	30°16.59'	35°17.11'	1313	90.1	0	0.0	0.0
516F	30°16.59'	35°17.10'	1313	1270.6	128	1101.5	691.7
517	30°56.81'	38°02.47'	2973	50.9	12	50.9	48.5
518	29°58.42'	38°08.12'	3944	76.7	19	76.7	59.6

^a All latitudes are south.
^b All longitudes are west.

proposed the concept of sediment transport by AABW to explain the similarity of distribution patterns of clay minerals in surface sediments of the Argentine and Brazil basins.

Site 516 was drilled at a depth within the present range of intersection of Upper Circumpolar Water and the seafloor (Reid et al., 1977; Barker et al., 1981). Our objective, to reach basement, was achieved after 19 days of drilling. The Rio Grande Rise was drilled twice during DSDP Leg 3, but spot-coring and shallow penetration at Sites 21 and 22 (Table 1, Fig. 2) only hinted at the history of sedimentation preserved on this topographic high (Maxwell, Von Herzen, et al., 1970a). As a result of Leg 39 drilling, much of the history of sedimentation was recovered at Site 357, although that site too was only spot-cored. Because basement was not reached, however, the questions raised by Maxwell and others (1970d) remained unanswered at the end of DSDP Leg 3 drilling: "Is the Rise a fragment of a continental crust left behind as South America drifted westwards? Or is it an oceanic basalt rising above the surrounding region as a group of seamounts or guyots?"

Sites 517 and 518 complete the transect: their water depths lie within the present-day depth ranges of North Atlantic Deep Water (NADW) and Lower Circumpolar Water (LCPW), respectively (Barker et al., 1981). The

present-day foraminiferal lysocline in the South Atlantic is near the upper surface of AABW (Berger, 1968). Should glacial-interglacial climate fluctuations influence the formation of AABW along the continental shelf of Antarctica (Newell, 1974), those changes in turn would alter the vertical profile and rate of flow of AABW in the area examined during Leg 72. Perhaps the upper surface of that water mass would rise to levels as shallow as the seafloor at Site 517. Ideally, such a fluctuation would be preserved in the sedimentary record as a dissolution pulse.

METHODS

Procedures for core handling and for the visual and smear slide examinations of Leg 72 cores follow the conventions established during previous DSDP voyages (Coulbourn, Explanatory Notes, this volume). A Rigaku X-ray diffractometer Miniflex (#2005), fitted with a Cu tube emitting $\text{CuK}\alpha$ radiation at 30 kV, 10 mA was newly installed aboard *Glomar Challenger* before Leg 70. Because the ship's electrical current has a frequency of 60 Hz and the X-ray diffraction unit and chart recorder are designed to operate at 50 Hz, the choice of scan speeds is 2.4 or 0.6° 2 θ /minute, instead of 2.0 or 0.5° 2 θ /minute. Accurate measurements of 2 θ are made by reference to the event marker box signal and not to the squares on the chart paper. Small variations in the rate of paper advance occurred. Leg 70 scientists advised using sylvite as an internal standard for calibrating chart speed. The diffraction peaks for sylvite proved a nuisance because the peak at 28.3° 2 θ is close to one for phillipsite, a coincidence that makes the diffractograms more difficult to interpret. The desired standardization is also achieved by adding halite, which only enhances peaks already present. Replicate analyses with and without halite produced the same diffractogram, halite peaks excepted. Accordingly, the use of sylvite was discontinued after a first series of analyses at Site 515.

Building upon the experience of the Leg 70 shipboard scientists, I produced the highest signal-to-noise ratios by crushing a small amount of sample that had been mixed with a few drops of distilled water and a small amount of Calgon in a mullite mortar until the slurry was homogeneous, then smoothing several drops of the slurry across a glass slide and drying the slide in a desiccator at room temperature.

The analyses reported here began with a few test runs to assess the reliability and reproducibility of output from the machine. Replicate analyses on single samples indicate that a smooth, moderately thick covering produces the strongest signal. The symbol “*” identifies replicate analyses of samples plotted in Figures 3, 4, 8, and 9. The samples were taken across a 1-to-2-cm interval and occasionally spanned con-

trasting lithologies. Sample identification follows standard DSDP format (Coulbourn, Explanatory Notes, this volume). When samples from the same vial produced different XRD patterns, interpretations of both records are presented.

As a matter of expediency, bulk samples were analyzed, because time constraints and the 2.4° 2 θ /minute speed used would render clay mineral separation more costly in time than the return of information would warrant. Even had it been desirable, the slower 0.6° 2 θ /minute speed could not have been routinely used because of a shortage of chart paper on the ship. Most samples were scanned from 50 to 3° 2 θ .

Because of the mismatch of the rate of chart advance and the grid-spacing on the paper, mineral identification by picking diffraction peaks was more difficult than might otherwise be the case. Fortunately, a set of mineral standards were on board, and samples of them were prepared as described above and analyzed several times to produce a reliable XRD for each. The graph recorded for each of these standards was in turn traced onto transparent film for comparison with diffractograms from Leg 72 core samples. Characteristic peaks were checked against tabulated key powder lines (Chen, 1977) to verify the accuracy of the diffractograms (Table 2). No attempt was made to cross-check XRD synonymy. In particular, samples were not treated with ethylene-glycol and scanned a second time to distinguish chlorite from montmorillonite, therefore the montmorillonite-match could also derive from chlorite (Carroll, 1970). The lack of swelling and the dark green-gray color suggest that some of the presumed montmorillonite in Site 515 samples is chlorite. In contrast, most montmorillonite-matched samples from Site 516 swelled noticeably after core splitting. As another example, Kastner (1981) mentions that the distinction between clinoptilolite and heulandite requires making XRDs before and after heat treatment and that, because this procedure “... was not carried out on all clinoptilolite reported in DSDP volumes, it is probable that heulandite is less scarce than implied.” Similarly, the mineral categories reported in this chapter might combine others under single headings.

Identifications were initially made on a presence-absence basis, but after some experience with these XRDs and after comparisons with visual core and smear slide descriptions, and with carbonate bomb results, it was clear that information about relative abundances could be extracted. The quantification of diffractograms attempted in this study is an approximative version of a method of mutual standards (Rex, 1970). Rather than determining peak area ratios (Biscaye, 1965), we matched the peaks in each sample's XRD with those of pure standards. A score of 5 indicates a visual match of characteristic peak heights between the standard and the unknown, and zero indicates a complete lack of match. A score of 1 is reserved for tentative identification, when the appropriate characteristic peaks barely rise above the background noise. Scores of 2, 3, and 4 indicate the standard is a rare, common, or abundant constituent of the sediment, respectively. For

Table 2. Mineral standards used during Leg 72 X-ray diffraction analyses.

Anhydrite				<u>25.52</u>	31.38	38.64	43.28		
Calcite				23.53	<u>29.37</u>	36.0	39.52	43.07	
Opal-CT				<u>21.4</u>					
Clinoptilolite	<u>9.83-9.91</u>	11.18	17.35	22.45	30.8				
Domolite					30.98	33.56	41.22	45.10	51.14
Feldspars		13.41-14.05		<u>23.53-23.79</u>	<u>25.52-25.82</u>				
Gypsum		<u>11.7</u>		20.80	<u>29.18</u>	31.16			
Halite				27.35	31.72		45.48	56.52	
Illite	<u>8.75-8.87</u>	17.73-17.81	19.81-19.95	<u>26.60-26.65</u>					
Kaolinite		<u>12.39</u>	20.36	<u>24.87</u>		36.06	38.46		
Magnesite						32.68	35.92	43.07	46.85
Montmorillonite	<u>7.12</u>			<u>19.86</u>	28.89				
Nontronite	<u>6.09</u>			<u>19.72</u>		34.91			60.95
Phillipsite		12.29	17.52	21.51	<u>27.96</u>	33.30			
Quartz				<u>20.85</u>	<u>26.68</u>		36.67	39.52	50.20
Serpentine	<u>12.00-12.46</u>			24.31-25.22			35.62-37.79	41.61-42.02	
Siderite				24.80			<u>32.07</u>	38.46	42.43
Sylvite					<u>28.33</u>			40.63	50.23
									66.44

Note: Numbers indicate respective diffraction peaks in degrees 2 θ ($\text{CuK}\alpha$, after Chen, 1977). Underlining indicates peak(s) most useful for identification.

Brazil Basin and São Paulo Plateau Sites

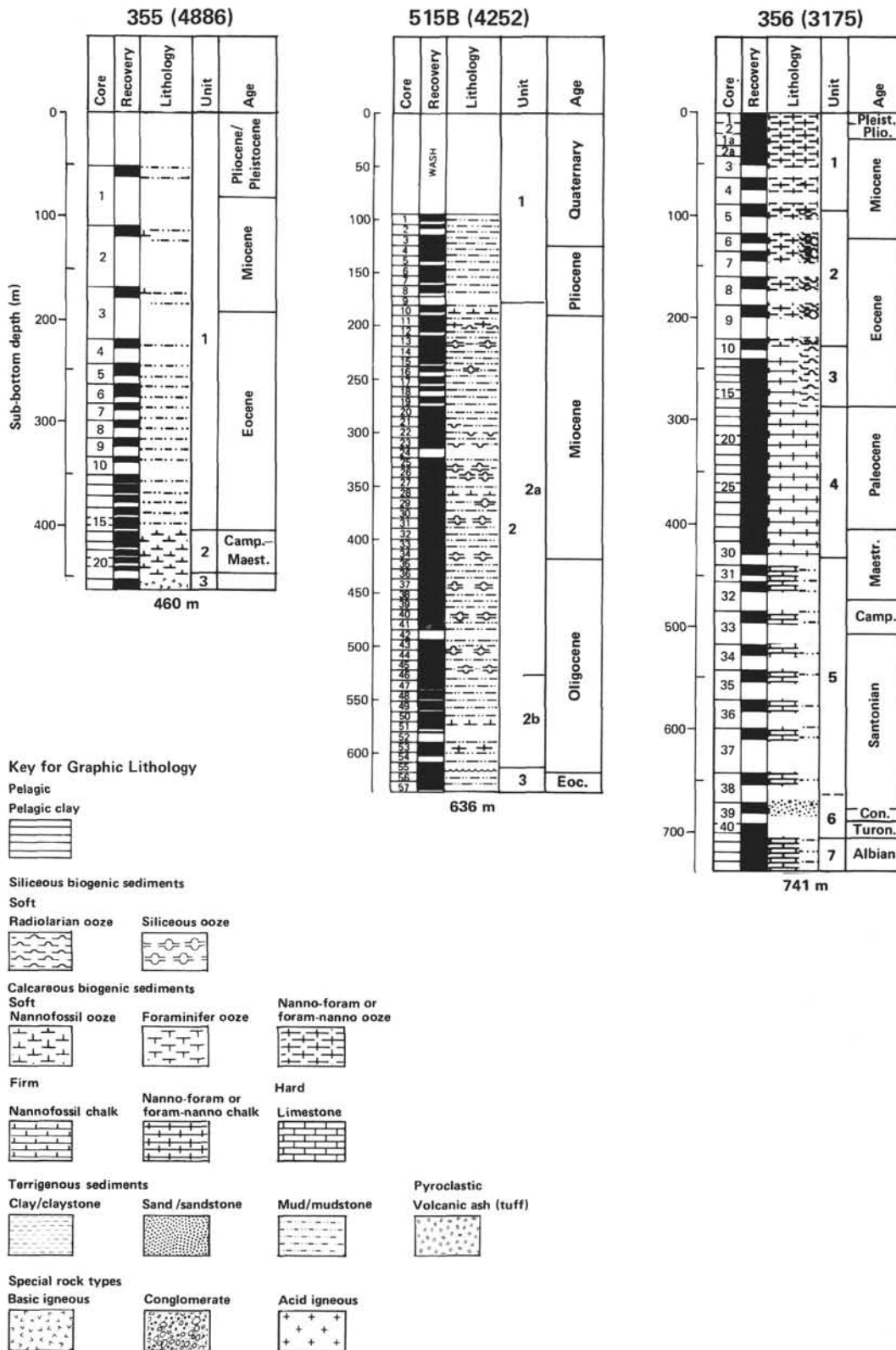
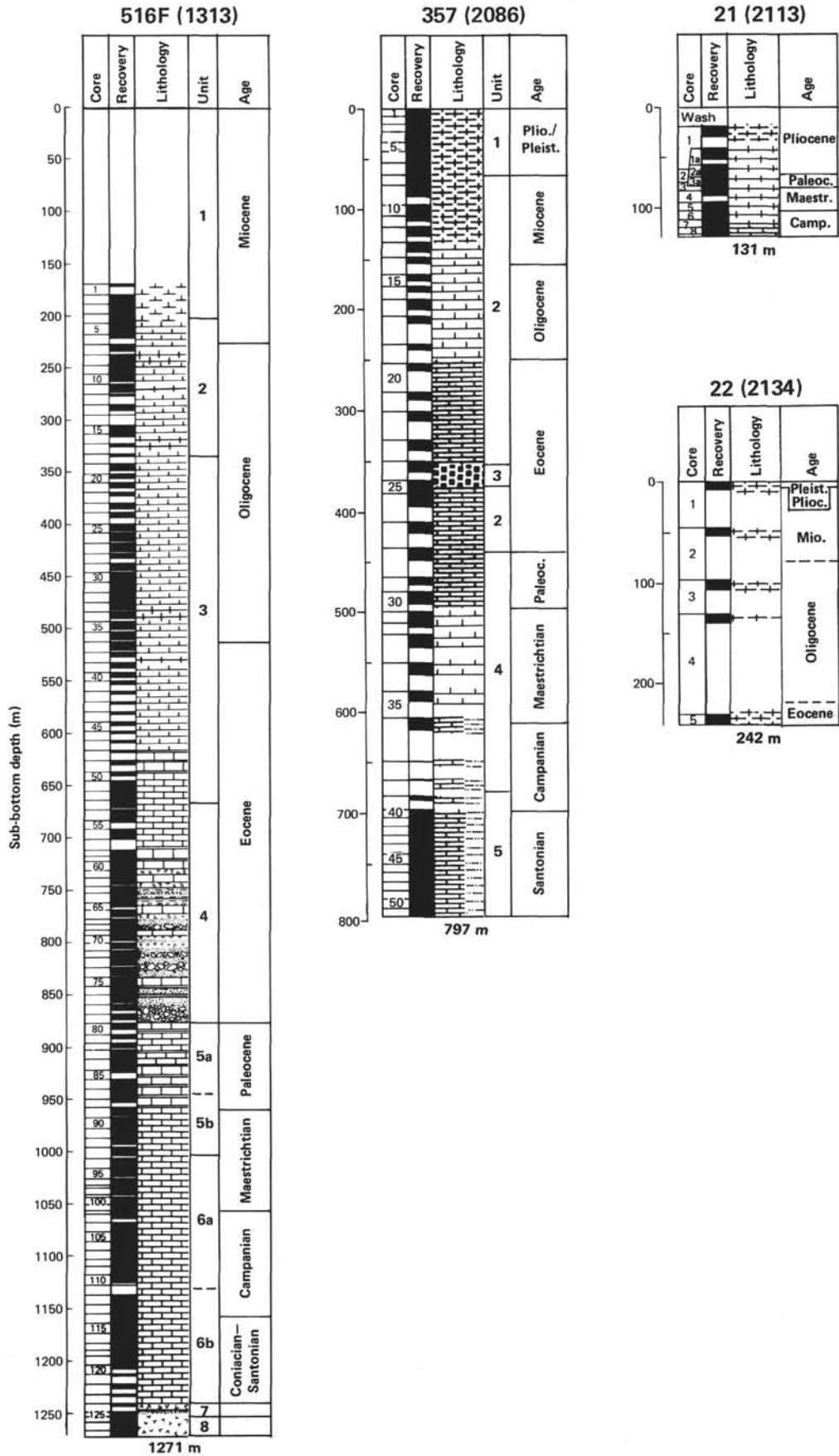


Figure 2. Summary lithology for southwestern Atlantic Ocean drill sites. Lithologic columns for Sites 21 and 22 are redrawn from Maxwell and others (1970b, c), those for Sites 355 to 357 are redrawn from Perch-Nielsen and others (1977a, b, c) and Scientific Party (1975); and those for Sites 515 to 518 are modified after the originals in Barker and others (1981). Water depth (in m) is shown in parentheses after each hole number.

Rio Grande Rise Rotary-cored Sites



Leg 72 HPC Sites

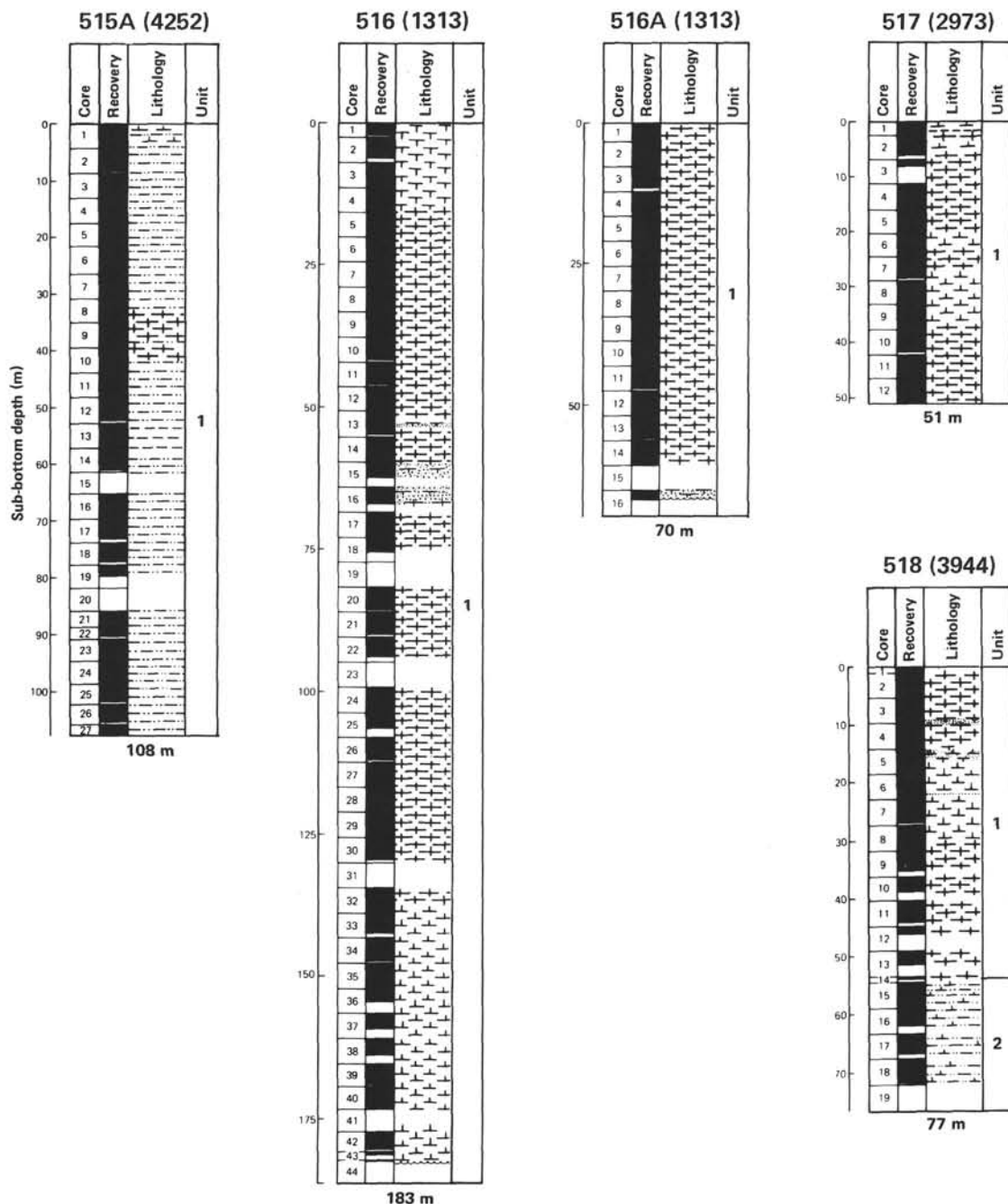


Figure 2. (Continued).

future projects, mixtures of known proportions of the standards should be X-rayed during the cruise; those diffractograms would improve the accuracy of these determinations.

In a few cases, peaks matched none of the standards available and these instances are recorded as an occurrence in the "other" category. Attempts were made to identify additional unknown minerals by comparison with key line tables (Chen, 1977) and with ASTM cards (American Society for Testing Materials X-ray Powder Diffraction File, Smith et al., 1960), and the results are described for those samples identified.

Description of lithology, and values for sonic velocity and carbonate bomb are taken from the core description forms (Sites 515 and 516 chapters, this volume) and from visual core description forms filed in the DSDP data bank. Those values plotted in this report are from measurements made close to and in a lithology similar to samples analyzed on the diffractometer.

Diffractograms for all samples are on file at the DSDP data library and copies of selected records are available on request to the Manager, DSDP data library.

SITE 515, BRAZIL BASIN

Background

Site 515 was continuously cored by the hydraulic piston corer (HPC) at Hole 515A to 107.9 m and by rotary coring at Hole 515B to 636.4 m sub-bottom (Fig. 2). Studies of suites of piston cores from near the Vema Channel have reconstructed a history of AABW flow for the past 1 Ma (Ellwood and Ledbetter, 1979). To extend this reconstruction, Site 515 was located far

enough to the north of the Vema Channel that the surrounding seafloor is within a regional depositional environment (Fig. 1), but close enough that the sediments accumulating there should include components transported from the Argentine Basin and "jetted" beyond the channel (LePichon et al., 1971; Lawrence, 1979). The redeposited component was thought to include indicators of AABW, but these particles were more elusive than expected (Site 515 chapter, this volume).

Major Sedimentation Patterns: Recent to Eocene

Since the early Eocene, sedimentation at Site 515 has been largely carbonate free (Figs. 3 and 4). Illite and quartz are the dominant components in the uppermost 170 m of gray-brown sediment, and feldspars and kaolinite are of secondary importance. Zeolites occur throughout the Site 515 cores: phillipsite in the Miocene

and younger sediments, and clinoptilolite in the Eocene sediments.

Although the distinction between Lithologic Units 1 and 2 (Fig. 2) was originally based on an increase in siliceous biogenic components alone (see Sediment Lithology, Site 515 chapter, this volume), the boundary is clearly reflected in the clay mineralogy. Illite and kaolinite abundances wane toward the base of Unit 1 as montmorillonite/chlorite becomes the dominant clay mineral in the gray-brown and dark green-gray sediments of Unit 2; quartz persists, and feldspars and phillipsite remain of secondary importance. An increase in sedimentation rates from about 10 to 40 m/Ma (see Fig. 10 of the Site 515 chapter, this volume) across the Unit 1/Unit 2 boundary probably is linked to the added input of detrital montmorillonite or perhaps to a precursor, volcanic glass (Griffin et al., 1968; Chamley, 1979). The subdivision of Unit 2 at Core 515B-47 is based on the disappearance of siliceous microfossils in Subunit 2b. Only an increase in calcite abundance, reflecting the selective sampling of light-colored nannofossil-rich layers, distinguishes the X-ray mineralogy of this interval. Displaced Antarctic diatoms, anticipated before the voyage, are either poorly represented or absent in Miocene and younger sediments, and siliceous microfossils are entirely absent in Subunit 2b (Site 515 chapter, this volume). Furthermore, as a result of Leg 39 drilling, Zimmerman (1977) found that "large amounts of well-crystallized illite, expected from an Antarctic source, are not being transported into the South Atlantic by AABW." The evidence for a change from quiescent pre-Eocene to vigorous post-Eocene circulation in southwestern Atlantic DSDP sites is preserved only in the form of a hiatus.

The unconformity at Site 515 is represented as a lag deposit recovered in Section 515B-55, CC (617.3 m sub-bottom, Fig. 5) and separates Units 2 and 3. The unconformity is synchronous with, but not direct proof of, the anticipated record of onset of AABW production at the end of the Eocene. It also represents a long span of time, at least 22 Ma (Site 515 chapter, this volume), much longer than anticipated before drilling. Examination of washed samples under a binocular microscope and of smear slides under a petrographic microscope reveals that the lag deposit is composed of subangular, fine, sand-size grains. Quartz, fish teeth, glauconite, biotite, and heavy minerals are among the components identified. Grain-size contrasts above this unconformity are generally absent, although fish teeth are concentrated at 541 m sub-bottom (Core 515B-47), and sedimentary features are rarely as pronounced as the small-scale flame structures and rip-up clasts shown in Figure 6A, providing little indication of strong bottom flow. In contrast, Unit 3, supposedly deposited under quiet, pre-AABW conditions, contains parallel and cross-bedding (Fig. 6B).

In visual aspect and in mineralogy, the lower Eocene mudstone of Unit 3 contrasts sharply with the overlying lithologic column (Fig. 4). Unit 3 sediments are rich in color contrast and *Zoophycos*, identified by sheetlike traces bearing spiral C-shaped rib patterns. The red to

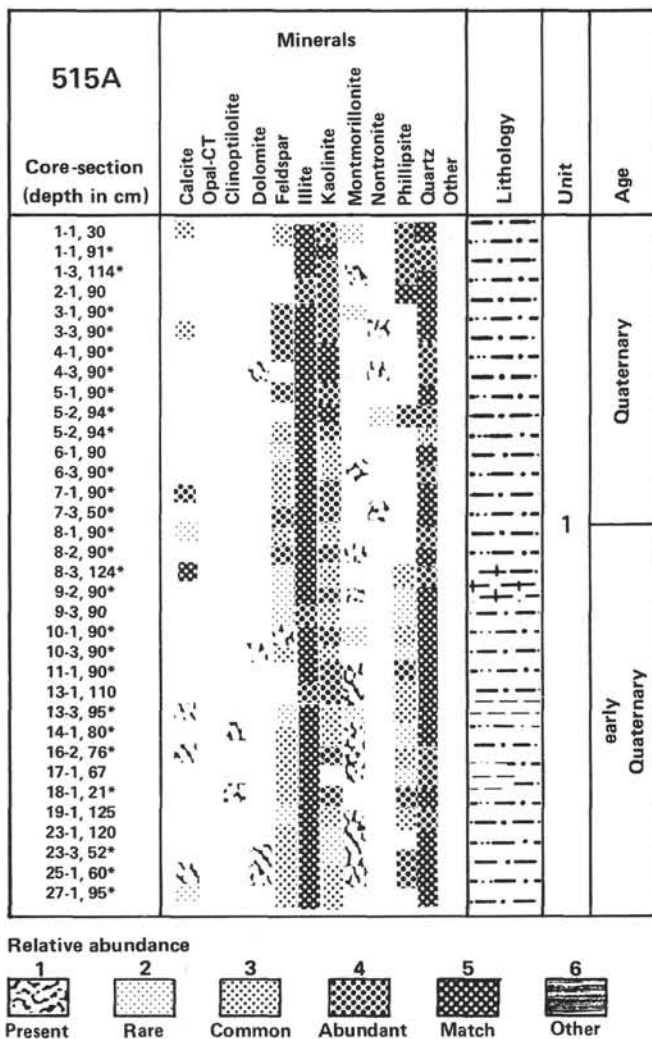


Figure 3. X-ray mineralogy of 34 bulk samples from Hole 515A. Lithology, unit description, and age assignment are from Site 515 chapter (this volume). Shading patterns refer to quality of match between standards and unknowns. XRD peaks not accounted for in the standards are identified as "other." * indicates replicate analysis.

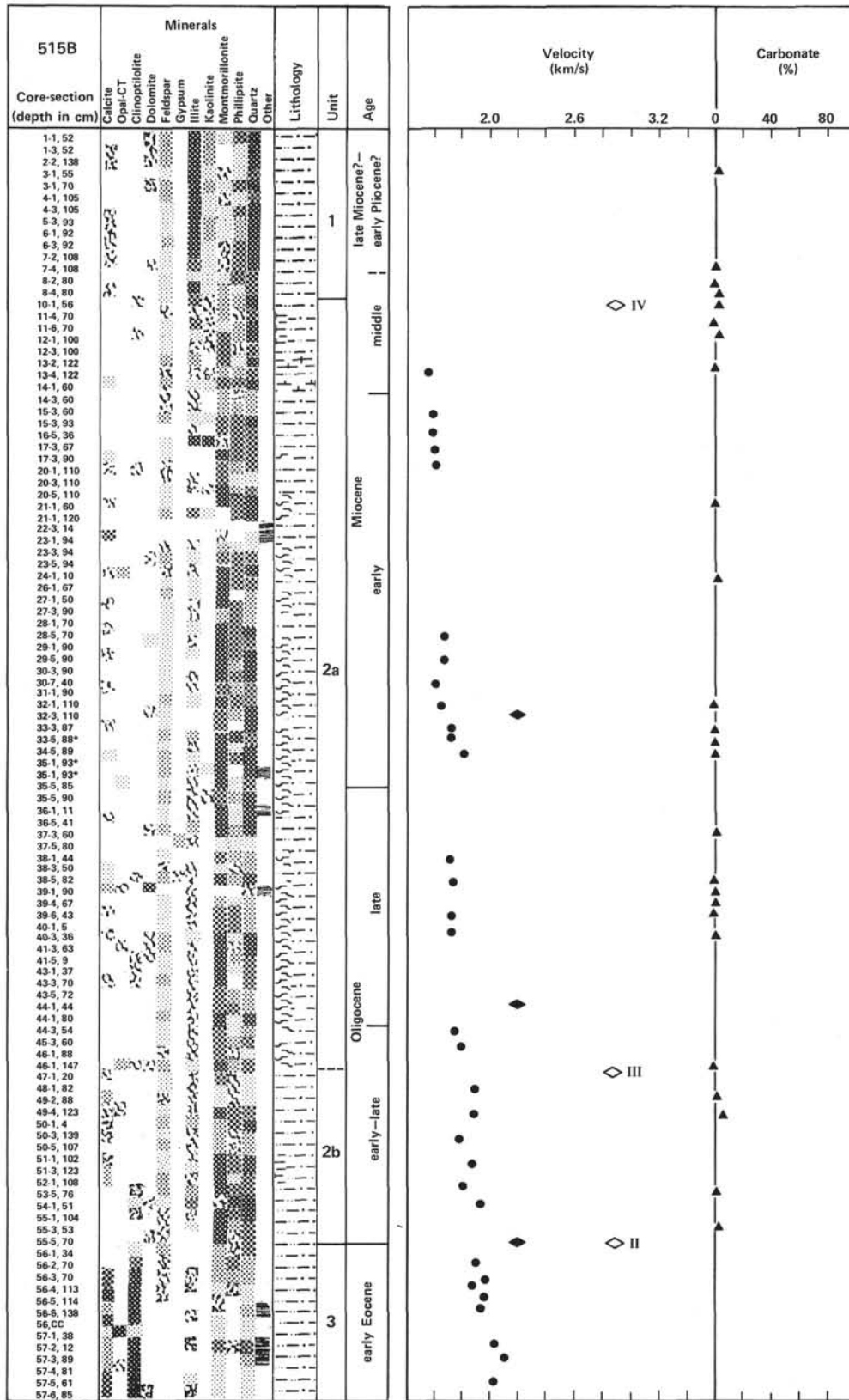


Figure 4. X-ray mineralogy of 108 bulk samples from Hole 515B. Lithology, unit designations, and age assignments are from the Site 515 chapter (this volume). * indicates replicate analysis. Shading patterns as in Figure 2. Sonic velocity and carbonate bomb values are selected from core descriptions (Site 515 chapter, this volume). Filled diamonds correspond to reflectors identified on a *Glomar Challenger* seismic profile made on the approach to Site 515. Roman numerals refer to regional seismic reflectors, which may represent erosional events (Gamboa et al., this volume).

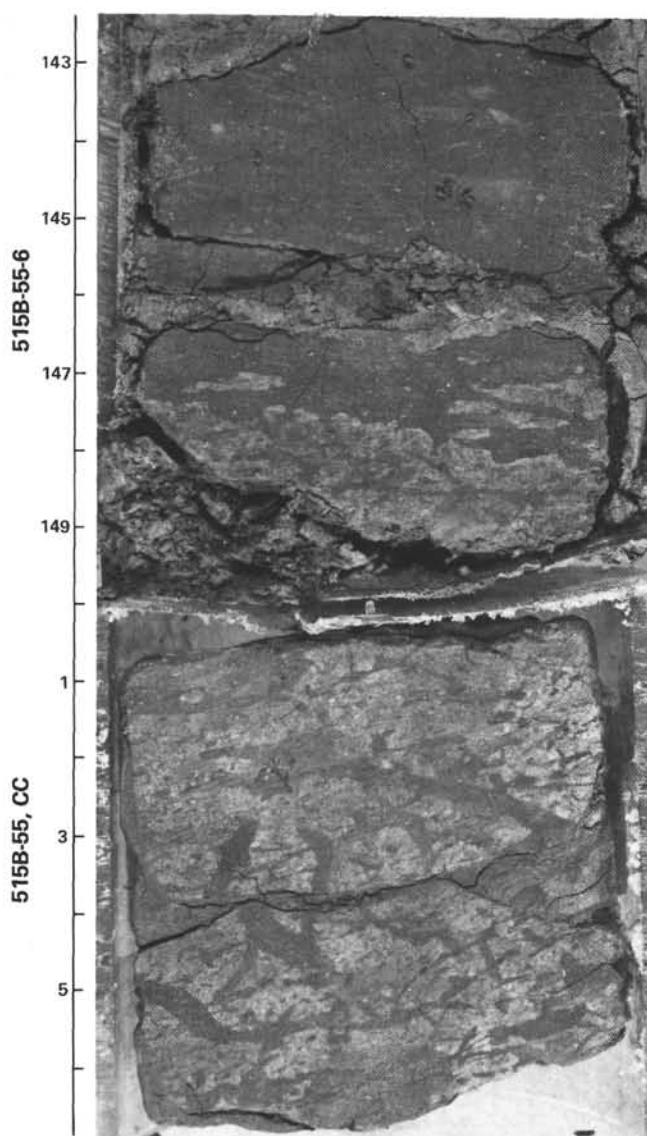


Figure 5. 515B-55-6, 145–160 cm and 515B-55, CC, lag deposit across Eocene/Oligocene unconformity.

green to black color range within Unit 3 bears little relation to the X-ray mineralogy at least at the scale of sampling for this report; clinoptilolite is dominant, calcite is of secondary importance, and a cherty horizon occurs in Sample 515B-57-1, 38–39 cm. The black layers are low in organic carbon but are biotite rich (de Quadros et al., this volume; Site 515 chapter, this volume). Emelyanov and Trimonis (this volume) found that clinoptilolite accounts for 15% of the sediment in a sample from Core 57, somewhat less than the patterns shown in Figure 4 suggest. In comparison to their visual contrast, the Unit 2 to Unit 3 transition in mineralogy is gradational, spread by benthic mixing over at least the first four sections of Core 515B-56. Abundances of montmorillonite, phillipsite, and quartz diminish gradually in the uppermost samples from Core 515B-56 as calcite and clinoptilolite abundances increase.

Minor Sediment Components

Minor components detected in XRDs of Site 515 samples include calcite, opal-CT, dolomite, gypsum, fluorapatite, and chamosite. Calcite is present in lighter-colored laminae, usually reworked between drill biscuits but occasionally preserved in some detail (Fig. 7B, C). Calcite concentration reaches a maximum of only 8% in levels corresponding to the X-rayed samples (Fig. 4), but the complete carbonate bomb record (Fig. 4 of Site 515 chapter, this volume) shows that carbonate “spikes” are more numerous and of higher amplitude than the points corresponding to the XRD samples might suggest, and this signal is the subject of another chapter (Shor et al., this volume). Opal-CT occurs in trace or low quantity in six samples from Unit 2 and is abundant in Sample 515B-57-1, 38 cm from Unit 3. Fluorapatite occurs in burrows in the intervals 515B-23-1, 94–96 cm, and 515B-39-1, 90–100 cm (Fig. 7A), and chamosite occurs in the spherules, perhaps originally ooids (James and van Houten, 1979) in Sample 515B-22-3, 14–15 cm. Gypsum was detected in Samples 515B-37-5, 80–81 cm and 515B-38-5, 82–83 cm; it also occurs in traces in DSDP Sites 136, 137, and 141 offshore of northwestern Africa (Berger and von Rad, 1972), and in piston cores from the Rio Grande Rise and Argentine Basin, in abundance in hemipelagic sediments at Site 495 (Prasad and Hesse, 1982), and preferentially concentrated in zones of strong CaCO_3 dissolution (Briskin and Schreiber, 1978). The occurrence of gypsum peaks in only two samples from Site 515 and the short time between core splitting and XRD analysis suggests that these occurrences are not artifacts of storage desiccation and preferential concentration of pore waters.

Relation of Mineralogy to Physical Properties and to Seismic Stratigraphy

Three sub-bottom depth intervals (400–420 m: Cores 515B-33 to 515B-35, 510–540 m: Cores 515B-44 to 515B-47, and 610–620 m: Cores 515B-55 to 515B-56) correspond to velocity changes responsible for reflectors observed on seismic profiles across Site 515 (Fig. 4, and Site 515 chapter, this volume). Of these, the relation between sonic velocity and mineralogy contrasts is apparent only for the Unit 2/Unit 3 boundary and only tentatively for the subdivision within Unit 2. Gamboa and others (this volume) correlate the seismic stratigraphy of the Brazil Basin with the lithologic section drilled at Site 515. Their seismic “Unconformities IV, III, and II” were drilled at Hole 515B (Fig. 4). Unconformity IV corresponds to the illite-montmorillonite dominance shift at the Unit 1/Unit 2 boundary. Unconformity III coincides with the Subunit 2a/Subunit 2b boundary, near a cherty sample that might be representative of a more extensive reflecting horizon. The stratigraphic break at the Unit 2/Unit 3 boundary is aptly termed “Unconformity II.” The reflector is synchronous with the late early to early middle Eocene Horizon A (Ewing et al., 1970), associated with clinoptilolite and montmo-

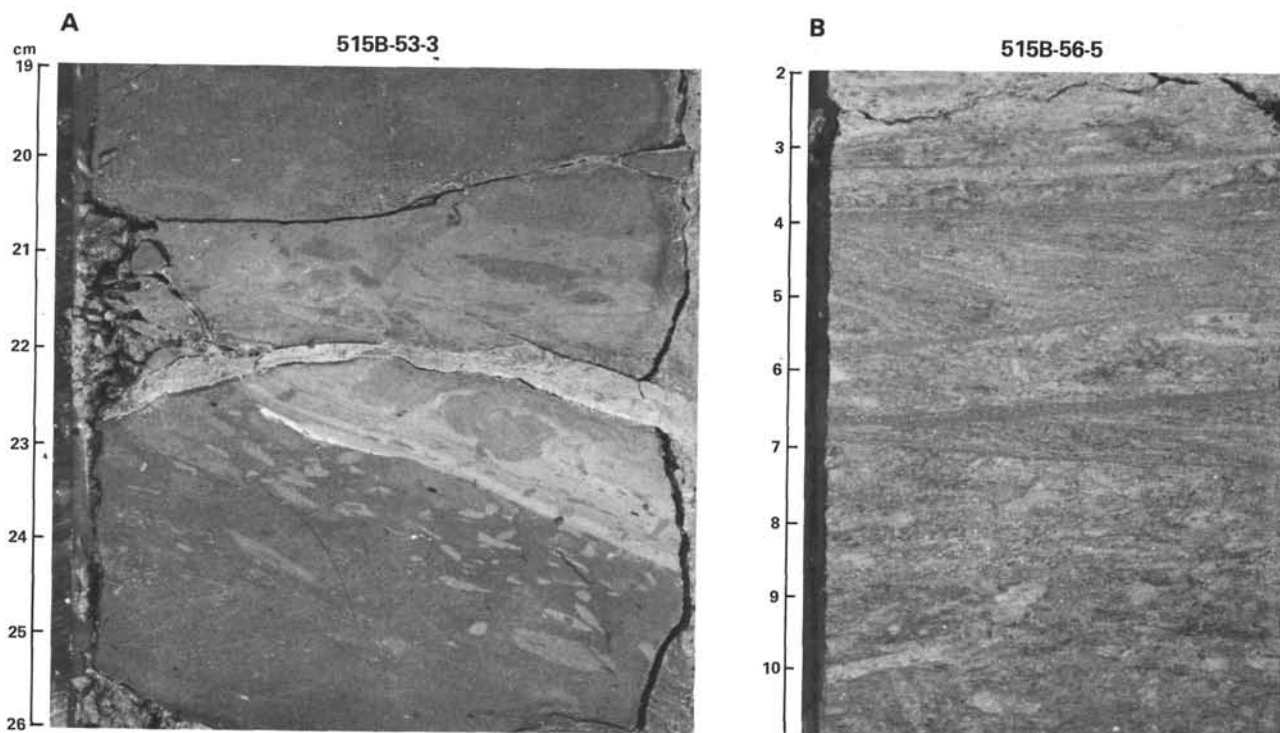


Figure 6. A. Section 515B-53-3, bed forms in Oligocene sediments. B. Section 515B-56-5, bioturbated, zeolitic mudstone typical of the Eocene sediments.

ronite occurrences over wide regions of the Atlantic Basin (for discussion see Kastner, 1981).

Comparison of Sedimentation at Sites 355, 356, and 515

A comparison of the lithology and X-ray mineralogy at Site 515 with results published in the *Initial Reports* for Leg 39 (Perch-Nielsen et al., 1977a, b, c; Zimmerman, 1977) indicates that the distributions match only in part (Fig. 2), and that most of the differences are probably related to geographic location. Few of the differences in results can be attributed to the analysis of carbonate-free versus bulk samples, because carbonate percentages are negligible in most Site 515 samples.

Although more distant, Site 355 bears a closer relation to the lithologic section drilled at Site 515 than do either Sites 356 or 357 (Fig. 2). Site 356 is located on the São Paulo Plateau edge at a depth of 3203 m, much shallower than Site 515, and the higher percentages of CaCO_3 reflect this depth difference. Sites 21, 22, and 357 are more appropriately compared to Site 516 because all are located in relatively shallow water on the Rio Grande Rise. Despite their disparate locations and depths, Sites 355, 356, and 515 all have unconformities separating zeolitic Eocene mudstones from overlying sediments. The hiatus is more pronounced at Sites 356 and 355, where it includes the upper Eocene and all of the Oligocene (Perch-Nielsen et al., 1977b) than at Site 515 where it spans 22 Ma between the middle Eocene and middle Oligocene (Fig. 2). Of the four sites drilled on the Rio Grande Rise (Sites 21, 22, 357, and 516, Fig. 1), an Eocene unconformity occurs only at Site 21, where some 45 Ma of sedimentation are missing (Maxwell et al., 1970d).

Site 355 is 640 m deeper than Site 515 and is considerably farther north (Table 1), but the low abundance of calcite at both locations underlines the first-order similarities of their lithology and mineralogy. Only three spot-cores represent the uppermost 220 m drilled at Site 355 (Fig. 2), and these Miocene and younger sediments are brown muds with carbonate proportions ranging between 0 and 10%, except in turbidites (Perch-Nielsen et al., 1977a). Illite is the dominant component in the uppermost sediments at Sites 355 and 515, and regional surveys show that illite and montmorillonite are generally the most abundant clays in Recent sediments of the South Atlantic Basin (Goldberg and Griffin, 1964; Biscaye, 1965; Griffin et al., 1968). Although illite dominates the clay mineral assemblage in piston cores from this portion of the southwestern Atlantic, sediments from deeper levels in Holes 355 and 515B indicate that this dominance does not persist downcore. Montmorillonite increases in importance in the Miocene sediments of both sites (Fig. 4; fig. 4 of Zimmerman, 1977). The biostratigraphic control for the timing of the illite-montmorillonite shift near the top of Core 515B-8 is very poor because Cores 515B-1 to 515B-7 are nearly barren of microfossils. According to the very tentative age assignments available (Site 515 chapter, this volume), that shift occurs 13 Ma earlier than similar patterns noted for North Pacific cores and related to Pleistocene glaciations (Jacobs and Hays, 1972).

Kaolinite is more abundant in the uppermost sediments at both Holes 355 and 515A than at Core V15-160 (Compare Fig. 3 with figs. 2 and 3 of Zimmerman, 1977). That difference reflects the relative proximity of Site 515 to tropical South America, a regional source of

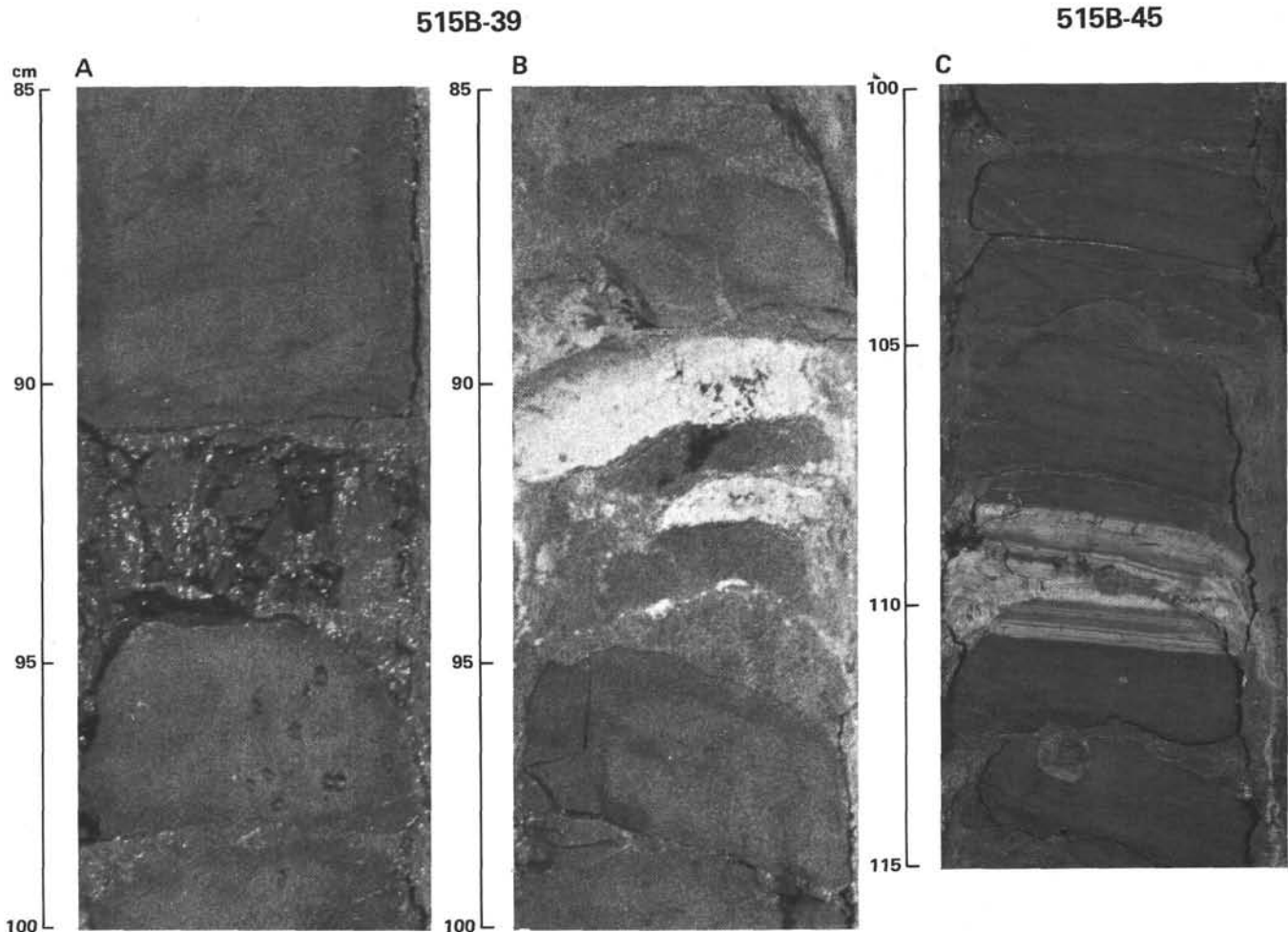


Figure 7. Details from Site 515. A. 515B-39-1, 85–100 cm; fluorapatite-enriched tube fillings. B. 515B-39-2, 85–100 cm, light-colored calcite-rich streaks remolded by rotary drilling. C. 515B-45-6, 100–115 cm, calcite-rich laminae in the dominantly carbonate-free sediments of Site 515 (see Shor et al., this volume).

detrital kaolinite (Goldberg and Griffin, 1964; Biscaye, 1965; Griffin et al., 1968). Concentrations of kaolinite are diluted by a relatively greater input of montmorillonite in Core V15-160, collected nearer to centers of regional volcanism and near to a latitudinal maximum of montmorillonite concentrations (Biscaye, 1965; fig. 2, Zimmerman, 1977).

Differences in lithology between Sites 355 and 515 arise mainly from the more important contribution of turbidites at Site 355. Differences in mineralogy occur mainly in the lower Eocene sediments. Although the alternately red-brown and green-gray zeolitic clays recall a like facies at Site 515 (Fig. 4), montmorillonite persists as the dominant constituent of Eocene sediments at Site 355 (Zimmerman, 1977). In contrast, montmorillonite is detected only sporadically in the calcite-clinoptilolite-dominated sediments of Unit 3, Site 515 (Fig. 4). Loss of the montmorillonite signal may result from dilution by calcite in these bulk sample analyses.

Patterns of Zeolite Accumulation

Zeolites are particularly abundant in the Brazil Basin, occurring throughout the Site 515 sedimentary section and at Site 355 (McCoy et al., 1977). The paragenesis of

zeolites in marine sediments is still somewhat of an open question, and various relations to diagenetic sources, companion lithologies, sedimentation rates, and formation ages are advocated.

At Site 515, phillipsite and montmorillonite co-occur in the Miocene and Oligocene sediments of Units 1 and 2 (Fig. 4). In a survey of zeolites of the world ocean, Kastner and Stonecipher (1978) found that phillipsite is associated with argillaceous, volcanic, and siliceous sediments, and also with montmorillonite; that association holds true for Site 515 sediments (Fig. 4). Apparently, Riech and von Rad (1979) found Stonecipher's (1976) association of phillipsite with comparatively young, slowly accumulating clays or volcanic sediments too restrictive. Their investigation of Leg 47A samples shows that the mineral is stable in Pliocene and Miocene sediments between 300 and 800 m sub-bottom and, in an interesting parallel with Site 515 calcareous turbidites (Shor et al., this volume), in sediments intercalated with quickly deposited calcareous oozes.

The phillipsite/clinoptilolite partition deduced from the XRDs of Site 515 samples (Fig. 4) could arise from a respective mafic versus silicic volcanic glass parentage (Petzing and Chester, 1979), but adoption of that view

relegates the remaining zeolite associations to the level of mere coincidence. Volcanic glass is present, however, only in low and trace amounts within Unit 3, supporting the view of Kastner and Stonecipher (1978) that a volcanic precursor for clinoptilolite in deep-sea sediments is unnecessary. McCoy and others (1977) noted that, although commonly associated with volcanic glass, clinoptilolite is also associated with biosiliceous remains and turbidites, each providing a source of silica for authigenic formation. Like volcanic glass, neither turbidites nor biosiliceous remains are important components of Unit 3 (Site 515 chapter, this volume), but opal-CT occurs in two samples (Fig. 4). This association favors Riech and von Rad's (1979) view that if, after complete dissolution of biogenic silica, the pore waters are undersaturated with respect to opal-CT, authigenic zeolites (among other phases) can be precipitated instead of opal-CT. Given that undersaturation, Cosgrove and Papavassiliou's (1979) computations of free energy of reaction indicate that within the sedimentary column clinoptilolite is stable with respect to phillipsite and could therefore form from phillipsite. Furthermore, diagenesis may have removed all visible evidence of precursors of clinoptilolite. Also possibly contributing to the partition of minerals at Site 515, clinoptilolite formation is reportedly enhanced in carbonate-rich sediments (Venkatarathnam and Biscaye, 1973; Kastner and Stonecipher, 1978; and Kastner, 1981); and calcite is the second most abundant mineral in the clinoptilolite-dominated samples constituting Unit 3 (Fig. 4).

A phillipsite-clinoptilolite relation to sedimentation rate has been described by Kastner and Stonecipher (1978): "... phillipsite-bearing sediments are generally deposited at rates of less than 5 m/10⁶ yr., whereas clinoptilolite-bearing sediments are generally deposited at rates of more than 5 m/10⁶ yr..." Such a relation is not evident for Site 515. The phillipsite-bearing sediments of Unit 2 accumulated at about 40 m/Ma, and the clinoptilolite-rich muds of Unit 3 at only 6 m/Ma (Fig. 4; Fig. 1 of Site 515 chapter, this volume).

The partition of zeolites with respect to time, the presence of phillipsite in the Oligocene and younger sediments, and clinoptilolite in the Eocene sediments of Site 515, corresponds well with temporal distribution patterns previously outlined (Venkatarathnam and Biscaye, 1973; Kastner and Stonecipher, 1978; Kastner, 1981).

SITE 516, RIO GRANDE RISE

Background

Site 516 was continuously cored to 1270.6 m sub-bottom (Fig. 2). The site was intended to sample sediments deposited beneath the upper levels of the southwestern Atlantic water column during a time interval spanning the Recent to the Cretaceous, and to decipher the subsidence history of the Rio Grande Rise. The latter goal was not achieved during Leg 3 because of spot-coring and mechanical difficulties, nor during Leg 39 at Site 357, because of lack of time. Because the column of sedimentary rocks was unexpectedly thick and many of

the Leg 72 objectives at other sites were still unfulfilled, the same failure was almost repeated at Site 516. Both objectives for Site 516 were eventually achieved by a combination of hydraulic piston coring at Holes 516 and 516A and rotary coring to basalt at Hole 516F (Table 1).

Major Sedimentation Patterns

Recent to Upper Eocene

In contrast with Site 515, sediments at Site 516 are dominantly carbonates (Figs. 8 and 9). Quartz and illite are of secondary importance in the foraminiferal-nanofossil oozes of Lithologic Units 1, 2, and 3. According to Emelyanov and Trimonis (this volume), illite accounts for about 5% of the sediment in the uppermost 200 m of the sediment column. A color change from pale brown and white to light gray downcore, increased quantities of sponge spicules, and thin green cherty laminations caused the shipboard sedimentologists to distinguish Unit 1 from Unit 2. The increase of feldspar in Emelyanov and Trimonis' (this volume) analyses of

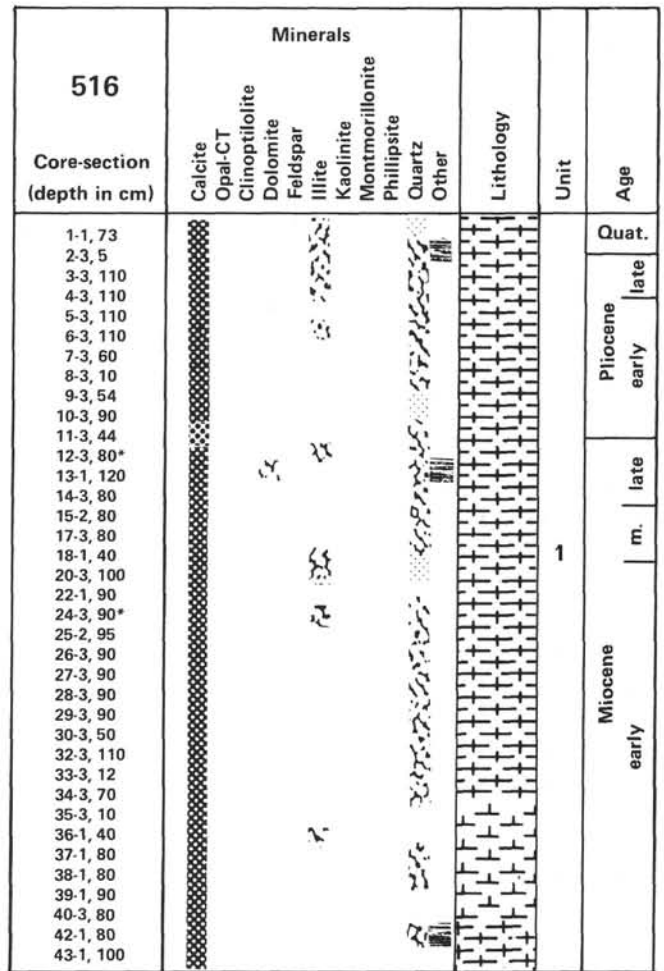


Figure 8. X-ray mineralogy of 37 bulk samples from Hole 516. Lithology, unit designation, and age assignments are from the Site 516 chapter (this volume). * indicates replicate analyses. Shading patterns as in Figure 3.

Unit 2 samples is not apparent in the shipboard XRDs. Because of the absence of a feldspar trend and failure to detect opal-CT in XRDs from Unit 2, the shipboard X-ray mineralogy offers no basis for distinguishing these two units. Continuing downhole, montmorillonite is detected in bulk XRDs in Unit 3, and the variety of the mineral assemblage sets this unit apart from the overlying 332 m of sediment. In general, the relatively homogeneous mineral assemblage of these first three lithologic units indicates that a stable sedimentary and diagenetic environment has persisted at Site 516 since the late Oligocene.

Middle Eocene Sedimentation and Events on the Rio Grande Rise

Stability is not typical of the Eocene segment of the geologic history of Site 516. A coarse sand bed, reworked downcore by burrowing (Fig. 8; Site 516 chapter, this volume) marks the top of this lithologic unit. Unit 4 is lithologically and mineralogically heterogeneous; Core 516F-68 serves as a good example (Fig. 10). Variability in grain size, bedform, and structure pervades this unit, and the individual members are too thin and varied to warrant division of the unit into subunits (Fig. 9). Occurrences of calcite, illite, and quartz are more sporadic in Unit 4 than above, but feldspar is more abundant. Dolomite occurs in three samples. Clinoptilolite, restricted to and so abundant in the Eocene sediments at Site 515, is barely detected in the calcite-rich sediments of the upper middle Eocene at Site 516. Montmorillonite abundance and the frequency of ash layers increase downhole in Unit 4. Emelyanov and Trimonis (this volume) report similar findings, and montmorillonite is also detected in all of Zimmerman's (this volume) analyses. These clays were recognizable visually, because immediately after core splitting they swelled rapidly above the level of the cut core surface. Diffractograms from most of the intervals identified as ash aboard ship do register high concentrations of montmorillonite, but some of the "ash layers" were later found to consist of detrital biotite (Bryan and Duncan, this volume). Those uncertainties notwithstanding, the montmorillonite at Site 516 most probably derives from the alteration of volcanic ash.

Chert, in addition to montmorillonite, is characteristic of the middle Eocene sediments from Hole 516F. Levitan and others (this volume) report the occurrence of quartz-cristobalite in Cores 4, 17, and 18, and porcelainite in Core 80. A chert nodule, approximately 1 cm in diameter, was found above Unit 4, at Core 516F-4-6, 120 cm (no XRD); and chert is reported in the smear-slide descriptions for Miocene and Oligocene Cores 5, 18, 21, 22, 23, and 33 (Site 516 chapter, this volume). For the most part these samples were from green laminations, their degree of chertification similar to that of the "incipient granular cherts" (Robertson, 1977). Not above Sample 516F-41-1, 77-78 cm does opal-CT occur in sufficient quantity relative to calcite to produce a distinctive peak in a bulk sample XRD. Opal-CT concentration increases markedly just below Core 41, the chalk-limestone transition, and is reflected as an increase in sonic velocity near Core 47 (634 m sub-bottom,

Fig. 9). Chertification here has proceeded as far as "Stage Three" (Heath and Moberly, 1971) in which silica has replaced, crystal by crystal, the radiating calcite prisms of foraminiferal test walls as well as the carbonate groundmass. As the frequency of occurrence of both opal-CT and ash layers diminishes from Core 77 to 81, so does sonic velocity, which shows a pronounced decrease near the Unit 4/Unit 5 boundary. Below Subunit 5a, quartz occurs in nearly every sample down to the base of Unit 6.

Feldspar is common in the interval between Sections 516F-75-5 and 516F-78-2 (Fig. 9), an indication of relatively rapid transport and burial. Other indicators of proximity to a shallow source abound. Oncolites, bryozoans, and nummulites and other larger foraminifers (commonly chertified) are reported in the visual core descriptions (Site 516 chapter, this volume). The combination of these microfossils, conglomerates, sandy intervals, dipping, graded and convolute beds, imbricated clasts, and faults are evidence for the uplift of the Rio Grande Rise during an episode of off-axis volcanism (Fig. 11, and Barker, this volume).

A slump, emplaced in the interval between Sections 516F-78-3 and 516F-79-4, heralds the middle Eocene rejuvenation of the Rio Grande Rise at Site 516 (Barker, this volume). In the process of moving to Site 516, the allochthonous red-brown, lower Maestrichtian limestones entrained pumice and a block of middle Eocene limestone, the aggregate now displaying steeply dipping beds, a variety of microfault patterns, and soft-sediment deformational features (Fig. 12). These characteristics and occurrences of illite and dolomite contrast sharply with the light gray limestones both above and below (Fig. 9). Their color and mineralogy resembles their time-equivalent sediments in Subunit 6a.

Paleocene Sedimentation and Flaser Limestones

Evidently the Paleocene was a time of considerably quieter sedimentation than was the Eocene at Site 516. Once again, as in Lithologic Units 1 through 3, calcite dominates and quartz and illite are of secondary importance in this white limestone (Fig. 9). Indicators of shallow water and tectonism so common in Unit 4 are rare in Unit 5. Ash beds and montmorillonite become rarer as illite becomes more abundant downhole, suggesting either quiescence of local volcanism, a relatively greater volume of terrestrial input, or conversion of montmorillonite to illite. Aoyagi and Kazama (1980) stress the importance of overburden pressure in the latter process; if the illite in Units 5 and 6 is diagenetic, this change has occurred at much shallower depths, around 860 m at Site 516 compared with 3500 m sub-bottom in the Japanese drill holes. Such an origin would imply that the now illite-rich marly interbeds were once montmorillonitic, and in turn that regional volcanism was not unique to the Eocene at Site 516. Furthermore, McHargue and Price (1982) relate the montmorillonite-to-illite transformation to dolomite formation in argillaceous carbonates, and that mineral does occur sporadically in Unit 5 samples. Diffraction peaks for dolomite become stronger and occurrences more persistent downhole in

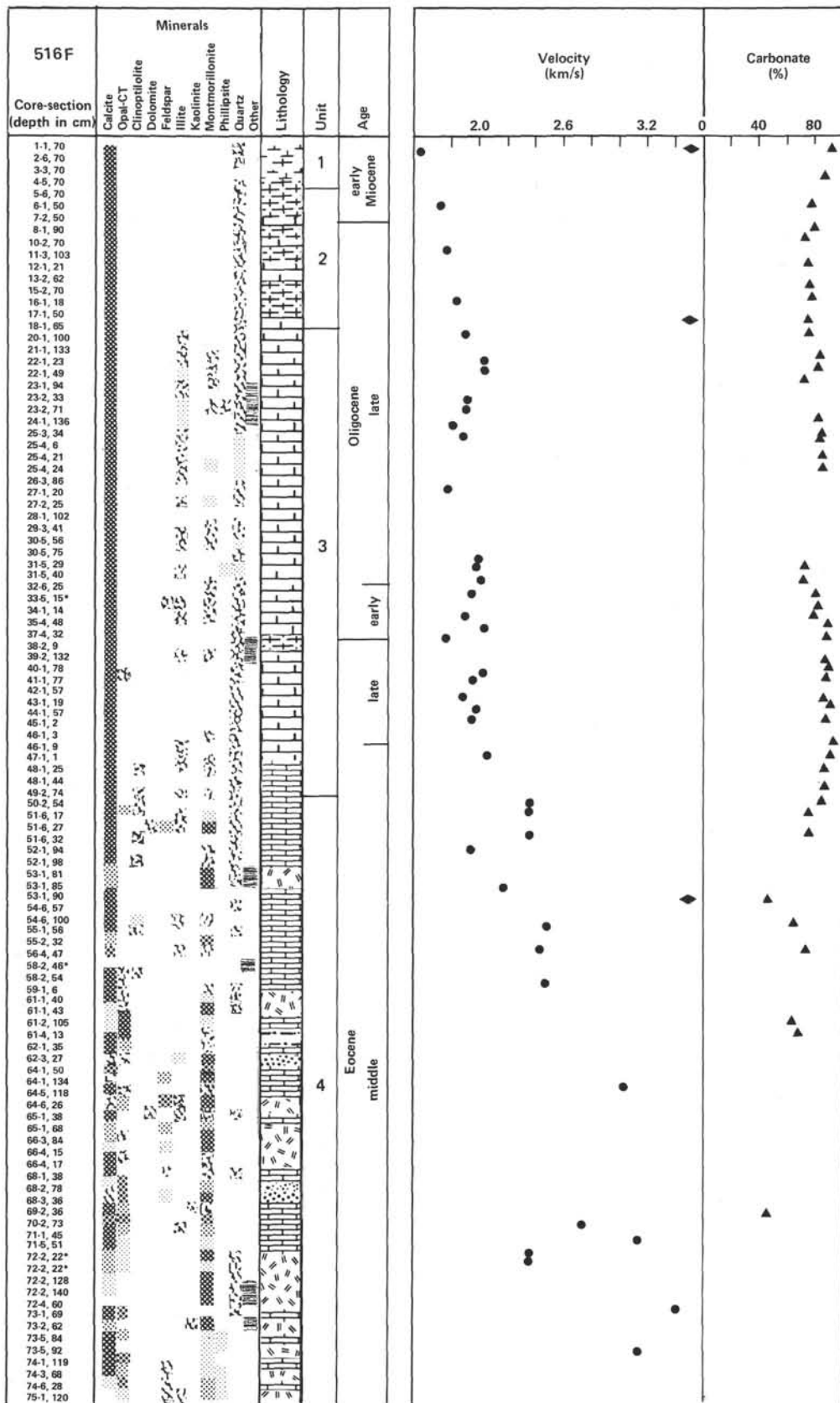


Figure 9. X-ray mineralogy of 218 bulk samples from Hole 516F. Lithology, unit designations, and age assignments are from the Site 516 chapter (this volume). * indicates replicate analysis. Shading patterns as in Figure 2. Sonic velocity and carbonate bomb values are selected from core descriptions (Site 516 chapter, this volume). Filled diamonds correspond to reflectors identified on a *Glomar Challenger* profile made on the approach to Site 516 and on multichannel profile WSA13 (Barker, this volume).

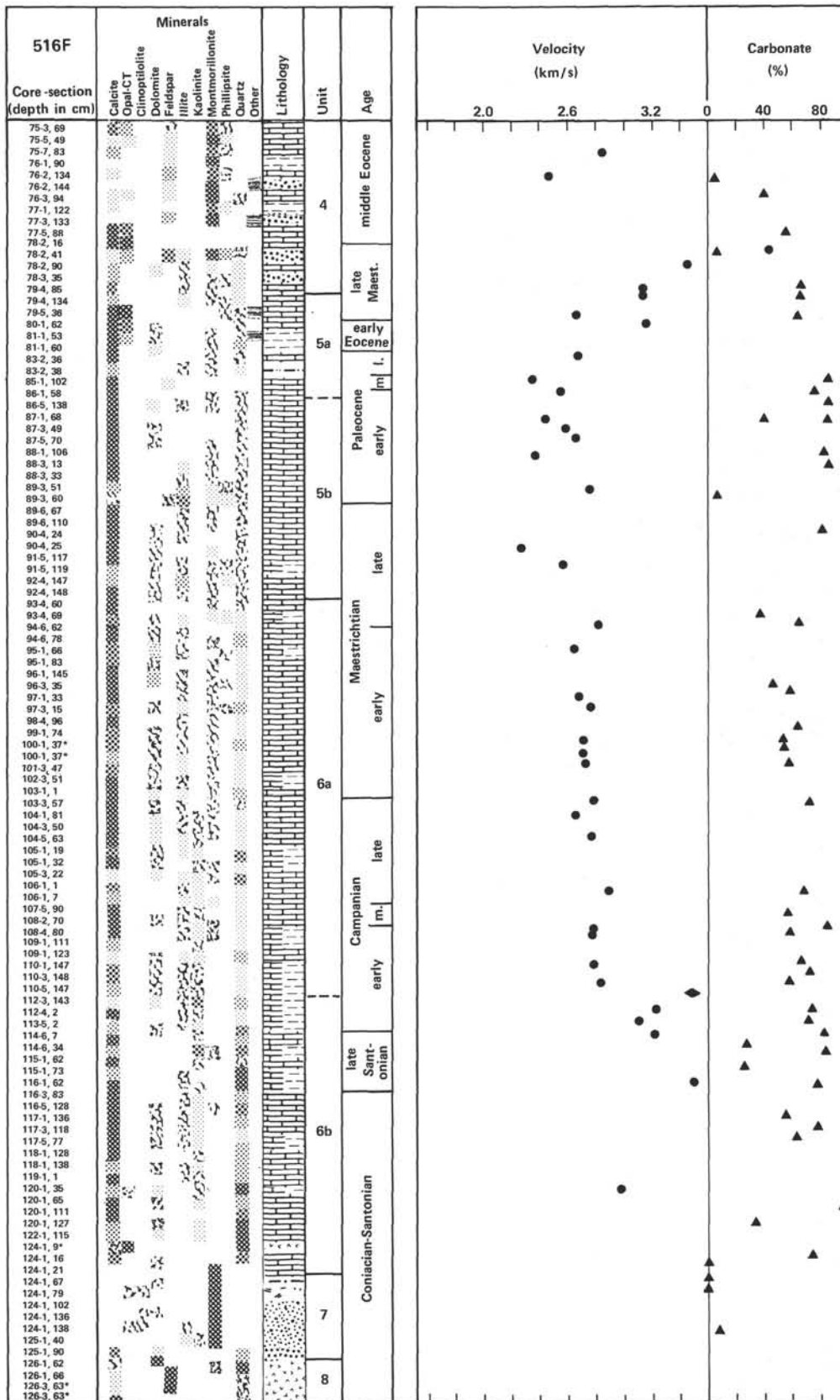


Figure 9. (Continued).

516F-68-3

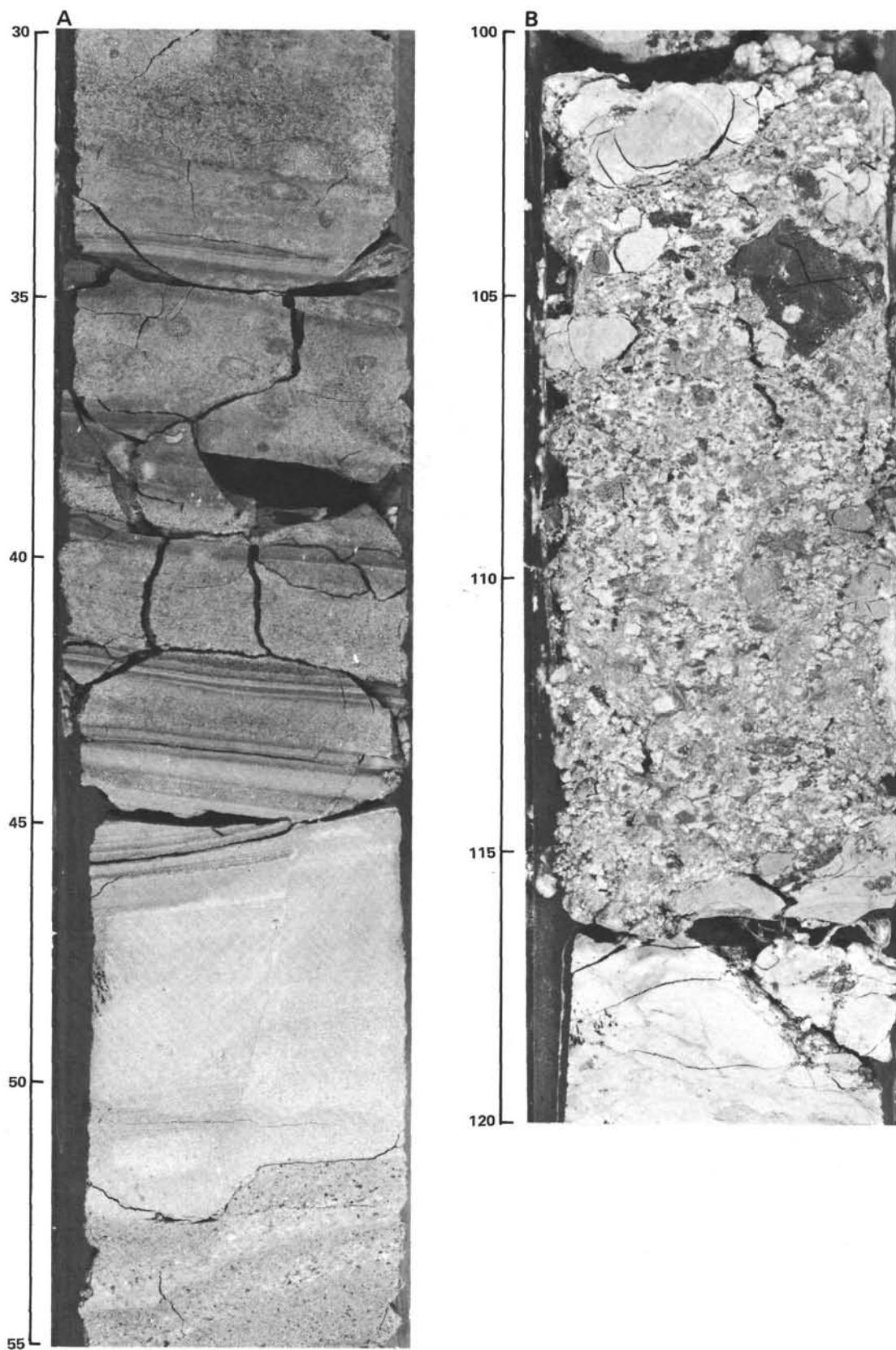


Figure 10. Heterogeneous grain size and lithology of portions of Sections 516F-68-3. A. Graded beds, offsets, and scour (516F-68-3, 30-55 cm). B. Breccia (516F-68-3, 100-120 cm).

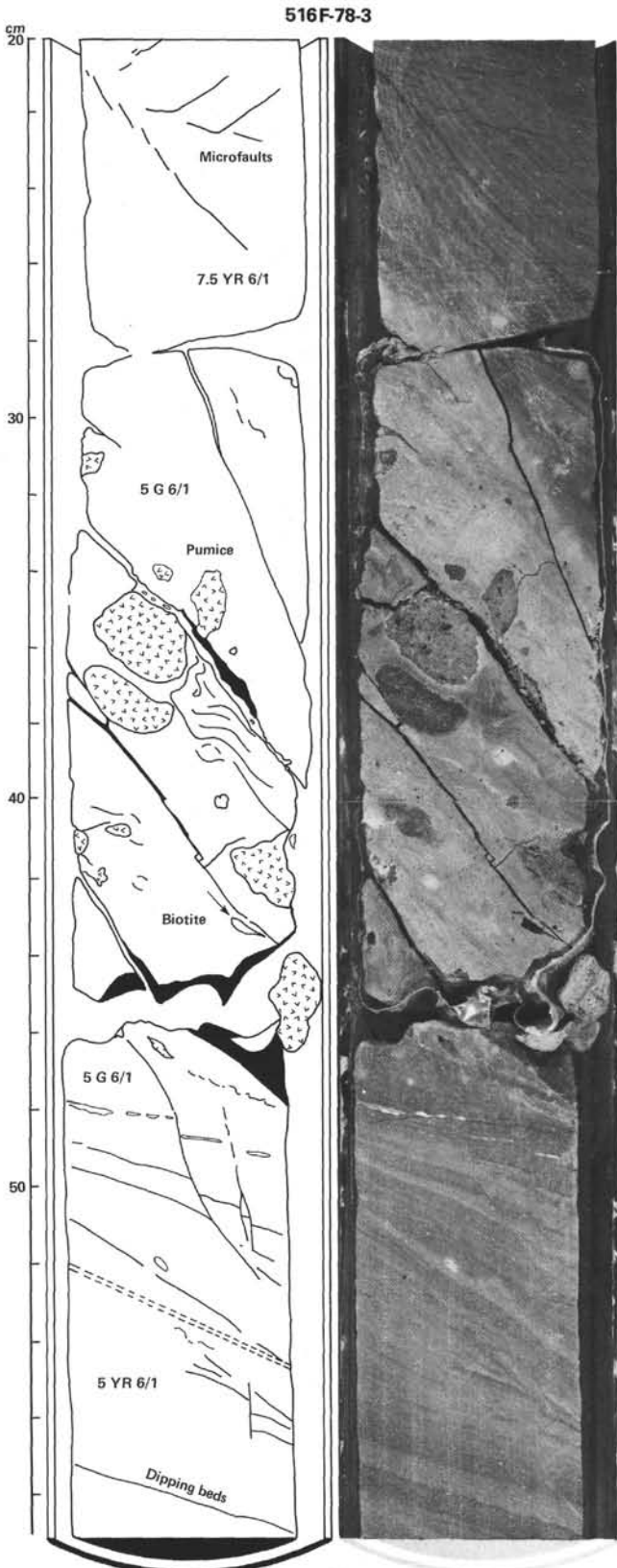


Figure 11. 516F-78-3, 20–60 cm. Photograph and interpretive drawing showing upper contact between light gray Eocene limestones and underlying red-brown Maestrichtian limestone, slumped from the flank of the Rio Grande Rise. Double broken line denotes sharp color change as indicated by Munsell code. Pumice clasts, biotite, open and healed fractures, dipping and convolute beds simplified from photograph.

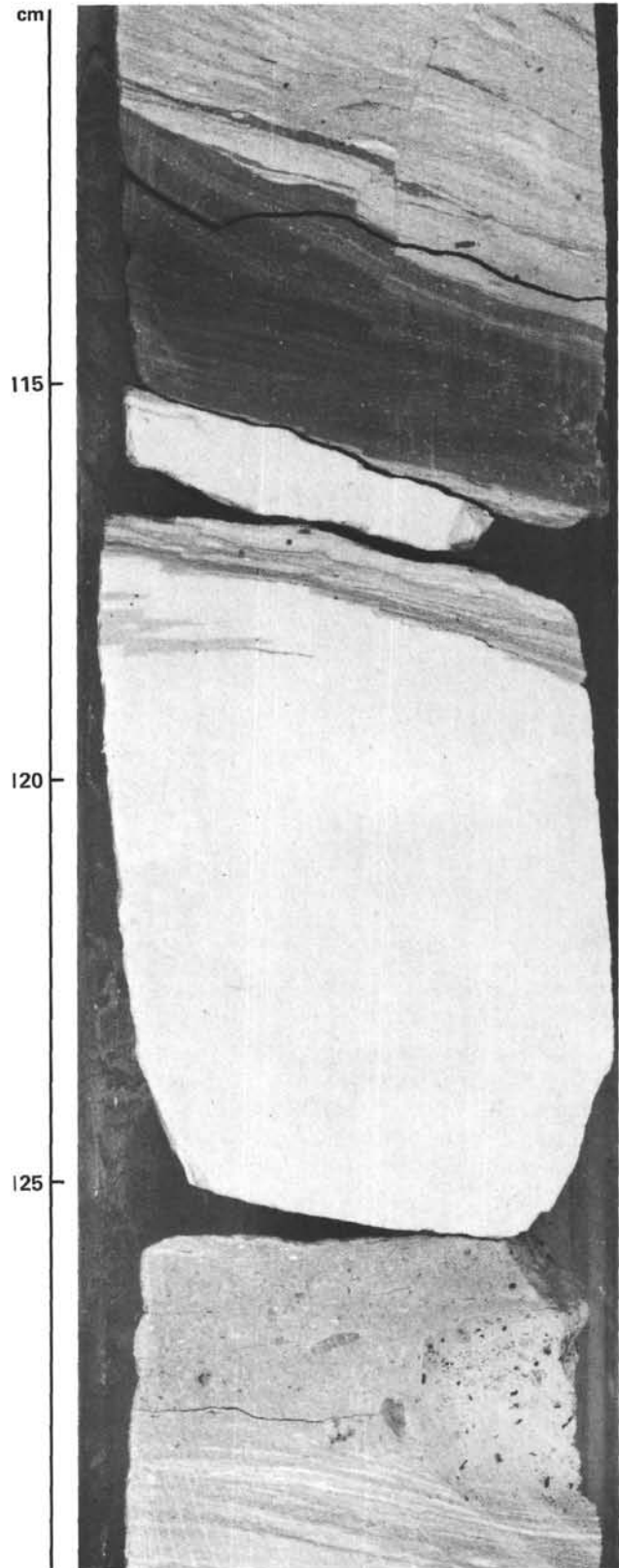


Figure 12. Interval 516F-78-4, 110–130 cm. A detail of the slumped mass occupying a portion of Lithologic Unit 4 (see Fig. 7, Site 516 chapter, this volume, for graphic overview). Offset, red-brown Maestrichtian limestone exhibiting soft-sediment deformation overlies white Eocene limestone. Gray Maestrichtian limestone beneath contains pumice clasts.

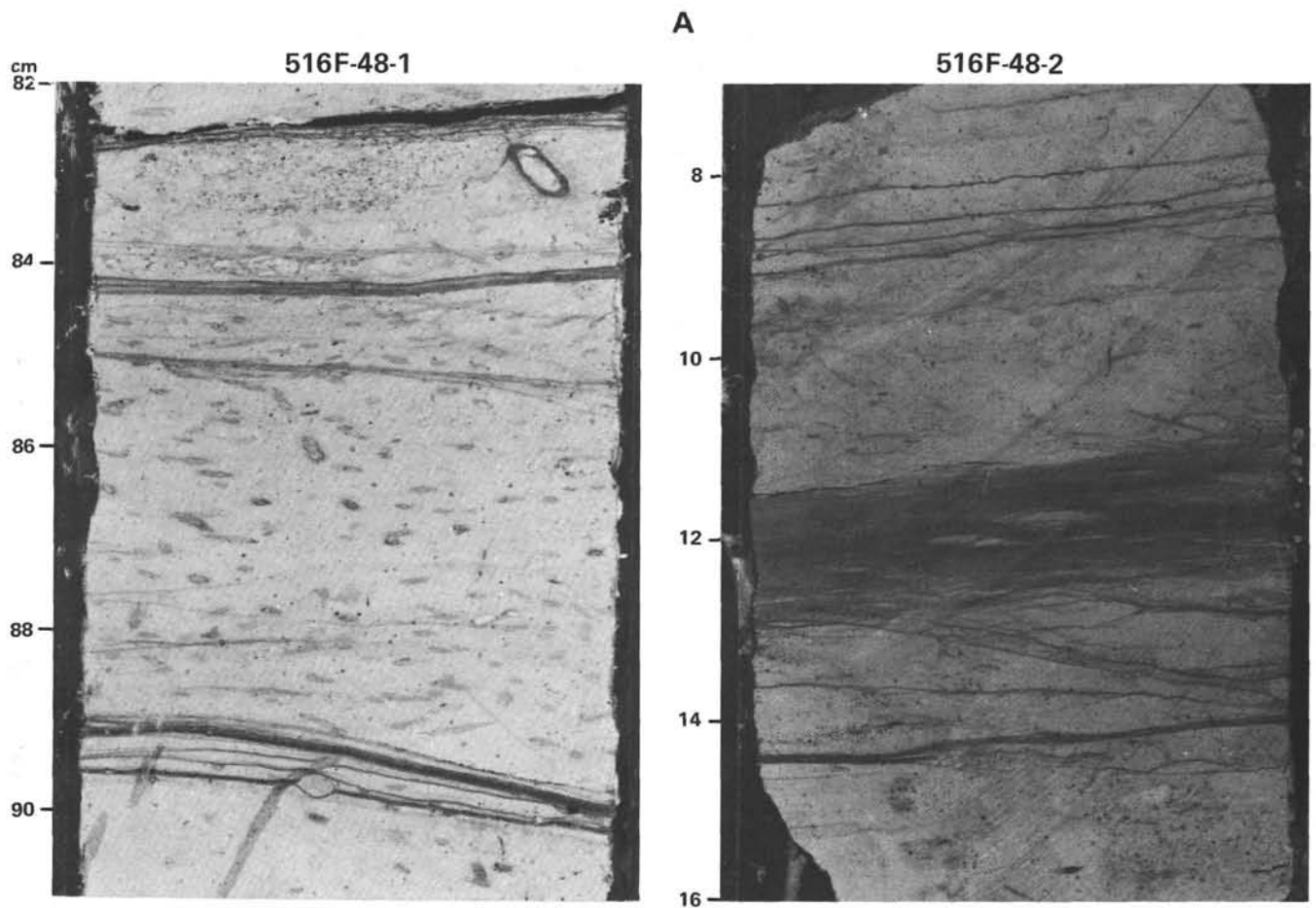


Figure 13. Examples of flaser chalks at Site 516. A. Trace fossils, laminations, and poorly developed flaser bedding in Core 516F-48. B. Lenticular bedding and nodular aspect of Core 516F-81. C. Nodular bedding in Core 516F-84. D. Flasers cut trace fossils and dark, illite-rich layers increase in thickness in Core 516F-86. E. Flasers and lenticular bedding and the Cretaceous/Tertiary boundary clay in Core 516F-89 (arrow indicates boundary location). F. Benthic mixing across marl-limestone contrast and waning of flasers as dark, marly intervals thicken in Core 516F-90.

Unit 6. Based on smear-slide observations made during Leg 72, dolomite occurs as isolated rhombs in Tertiary sediments and both as rhombs and as void fill and/or replacement in the Mesozoic micritic limestones, but no attempt was made to quantify the amount of each form present (Site 516 chapter, this volume). The limestones of Units 5 and 6 are deep water deposits. Only the dolomite in Sample 516F-126-1, 62–63 cm is associated with shallow-water microfossils and can be attributed to formation at a shallow depth of burial.

Associated with the appearance of dolomite peaks in XRDs from Unit 5 samples are wavy, illite-rich laminations within the limestone matrix (Fig. 13), features referred to as stylolites (Site 516 chapter, this volume). Although these features are related to pressure solution, a review of nodular pelagic limestones (Ogg, 1981) suggests that they are better referred to as flaser limestones (Garrison and Kennedy, 1977). As bedforms, the geometry of flaser and wavy beds arises from the supply of both mud and sand during periods of alternating current flow and quiescence (see fig. 169, Reineck and Singh, 1975). At Site 516 the contrast is related to size differences between mud and sand, but is probably not a bedform created as a direct response to bottom currents. The Site 516 flaser limestones are a small-scale

analog of the red nodular limestones of Sicily (fig. 2, Jenkyns, 1974) and closely resemble the middle Chalk from the Isle of Wight, England (fig. 8, Garrison and Kennedy, 1977). A search through the Leg 72 core photographs reveals that the flaser structure occurs at least as high in the section as Core 516F-48 (Fig. 13A). Those in Section 516F-48-1 were described as solution planes and those in 516F-48-2 as parallel laminations. These features closely resemble the pale green laminations occurring throughout the overlying 625 m overburden. Although uncommon in the upper and middle Eocene at Site 516, these “laminations” become characteristic of the lower Eocene and Paleocene (Fig. 13B–D). Their nodular aspect is clear in Core 516F-81 (Fig. 13B) as is their wavy pattern in Core 516F-84 (Fig. 13C). As the supply of clay increases downhole approaching the deeper levels of Subunit 5a and Unit 6, the flaser beds flatten and coalesce, becoming wavy bedding (Fig. 13D–F). These argillaceous layers, or solution seams (Garrison and Kennedy, 1977), generally parallel bedding and occasionally cut primary structures and burrows (Fig. 13D), indicating that the formation of the flaser structure occurred during late burial diagenesis.

The sub-bottom depth of formation of these features is uncertain. Indurated carbonates occur on the seafloor

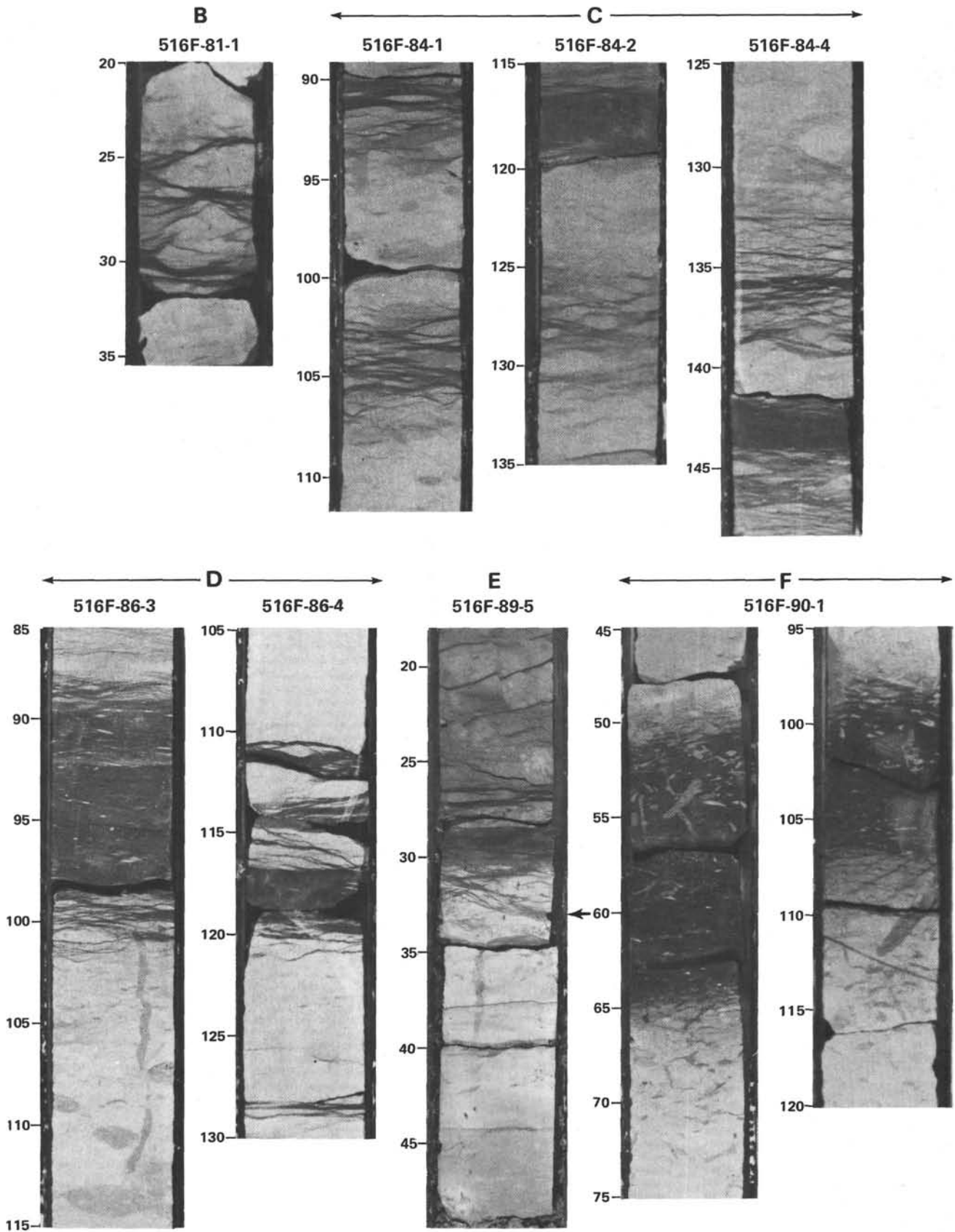


Figure 13. (Continued).

(Fischer and Garrison, 1967), and the carbonate-rich nodular limestones reported from the Bahamas are within piston-coring range of the seafloor (Mullins et al., 1980).

The mode of formation of these features is also uncertain. Although not creating the primary wavy bedform of the flaser structure, bottom current fluctuations over an appropriate velocity range would control the ratio of illite versus calcite deposited on the seafloor. Currents are considered important in creating an environment favorable to nodule formation on Bahamian slopes at present (Mullins et al., 1980). Those nodules occur preferentially between 400 and 600 m water depth, where currents "winnow about half the muddy sediment... and bioturbation is active." Stronger currents winnow all the mud, leaving continuous, well-lithified carbonates. Likewise, weaker currents allow soft unlithified oozes to accumulate by deposition of clayey sediment, which in turn decreases permeability and inhibits circulation of pore waters, preventing nodule cementation (Mullins et al., 1980). At Site 516, therefore, the increased quantities of clay occurring downhole in the Maestrichtian section would suppress nodule formation deeper in the section. How much of the flaser structure is a result of interstratal solution transfer of carbonate from the marly interbeds to the limestone also remains undetermined. Perhaps much of the flaser structure has little to do with primary layering, an opinion advocated by Wanless (1979), but the transition from flaser to bioturbated, marly interbeds in the Maestrichtian cores (Fig. 13D-F) is a clear indication that the basic alternating lithology was at least partially in place before pressure solution occurred. Whatever the origin of these features is, the selection of samples representative of the limestone and marl end members of the flaser structure produces the fluctuations in relative abundance of calcite, quartz, and illite, and also the scatter in carbonate bomb data (Fig. 9). For the most part, the marly beds are too thin to record and as a result are underrepresented in the very general summary lithologic column of Figure 9.

Cretaceous/Tertiary Boundary

The Cretaceous/Tertiary boundary occurs in Core 516F-89-5. Nannofossil biostratigraphy places the boundary at 33.5 cm, but foraminiferal assemblages indicate it is somewhat higher, between 21 and 26 cm (Site 516 chapter, this volume). The presence of all nannofossil and of all foraminiferal zones indicates continuous sedimentation across the era boundary at Site 516. The lithology of this interval is a continuation of the flaser and wavy bedded alternating limestone and marly limestone sequence described for the Paleocene cores, all grouped together in Lithologic Subunit 5b (Fig. 9). A typical "boundary clay," as at Site 524 for example (Hsu et al., 1982; Officer and Drake, 1983), is lacking at Site 516 (Fig. 13E). A 0.2-cm thick marly layer does occur at the nannofossil boundary, but it is only a part of the general flaser bedding characteristic of a wider stratigraphic interval. A comparison of the iridium abundance curve (Michel and others, this volume) with the lithology

shown in Figure 13E supports Officer and Drake's (1983) contention that abundance of this element is correlative with clay content. An iridium anomaly occurs between 16 and 36.5 cm with a maximum abundance coincident with the nannofossil boundary at 33.5 cm. Because of the biostratigraphers' need for samples across the boundary, no shipboard XRD analyses were carried out on samples from Section 516F-89-5. Rampino and Reynolds' (1983) XRD analysis of boundary clays from other locations around the globe shows no anomaly in the mineral assemblage. Based on appearance alone, no sedimentary feature gives reason to expect an anomalous XRD signal at the Site 516 Cretaceous/Tertiary boundary either. Nor is a special shoaling of the calcite compensation depth (CCD) or a surface-water productivity drop required to produce the marly interval near the boundary, unless these processes are invoked for each of the many marly intervals of this sequence.

The Mesozoic at Site 516

Changes in the mineral suite at Site 516 are only generally coincidental with the era boundary. Progressing downhole, illite and quartz concentrations begin increasing in Subunit 5b, as the number of marly intervals increases. Opal-CT concentrations diminish between Unit 4 and Subunit 5a, as distance (downhole) from the ashy horizons of Unit 4 increases. As silica concentration decreases, dolomite becomes notably more abundant in the Mesozoic deposits, a pattern supportive of Baker and Kastner's (1981) experimental findings that opal-CT formation suppresses dolomite crystallization. A relation between dolomitization and microbial sulfate reduction (Baker and Kastner, 1981) remains untested at Site 516 because of the paucity of organic carbon analyses (Site 516 chapter, this volume; de Quadros et al., this volume). With the exception of this opal-CT-to-dolomite diagenetic shift, which occurs gradually rather than at a sharp front, a uniform mineral suite characterizes the Paleocene and Maestrichtian sediments at Site 516.

Quartz increases in abundance near the top of Unit 6 as *Zoophycos* traces become more numerous (Fig. 9). Kaolinite appears in the Campanian and characterizes the lower half of Subunit 6a and most of Subunit 6b. Within Unit 6, diffractogram peaks for kaolinite gradually increase in height downhole, as those for illite decrease, and the color within Unit 6 changes from an alternating sequence of green-gray and dark red-brown stains in Subunit 6a to mostly dark gray in Subunit 6b. A second increase in abundance of quartz (Fig. 9) coincides with the color change and with the appearance of *Inoceramus* in Subunit 6b. These macrofossils are clearly visible in the cut cores and frequently extend across the entire core diameter (Fig. 14). Although Unit 6 generally lacks the variety and pervasiveness of structures found in Unit 4, these limestones do exhibit offsets and soft-sediment deformation (Fig. 15).

A ferruginous chert at the top of Core 516F-124 (Table 2 of Site 516 chapter, this volume) closely resembles Berger and von Rad's (1972) "Type 4" chert and marks Lithologic Unit 7, the interval from 516F-124-1, 30 cm to 516F-125-2, 30 cm (Figs. 9 and 16). The succession of

516F-114-5, ~128 cm



Figure 14. Plan view of *Inoceramus*, 516F-114-5, ~128 cm.

lithologies in these two cores is remarkable in variety. Ash beds, sand and graded beds, conglomerates, and breccias signal proximity to a shallow volcanic source, and basalt was recovered in Core 125. Ash and clay beds in Cores 124 and 125 contain the record of volcanism immediately following formation of crust at the Mid-Atlantic Ridge. Along with montmorillonite, opal-CT recurs and clinoptilolite is present, the same mineral association as in the Eocene (Fig. 9). Carbonate and quartz decrease markedly from their concentrations in Unit 6.

The olivine-plagioclase-phyric, tholeiitic basalt of Core 516F-126 encloses a large vein filled with quartz, calcite, and dolomite (Fig. 17). Clays and iron oxides fill small vesicles. Fragments of *Inoceramus*, coralline algae, and bryozoans are suspended in a matrix of sparite and micrite, the whole colored a translucent blue and white. If the Rio Grande Rise was not above sea level at the time of its formation, then it was close to it, the sea-floor lying within the photic zone (Milliman, this volume; Barker, this volume).

Minor Sediment Components

Minor components detected in XRDs of Site 516 samples include olivine, siderite, hypersthene, tridymite, and barite. Identifications of these minerals were made with

varying degrees of confidence and are listed together under "others" (Fig. 9). Olivine produces a peak at $31.6^\circ 2\theta$ (Chen, 1977) in bulk XRDs from Sections 516F-23-2, 516F-24-1, 516F-38-2, and 516F-39-2 (Fig. 9). Peaks at $13.5^\circ 2\theta$ for Samples 516F-53-1, 81–82 cm and 516F-53-1, 85–86 cm remain unidentified. The XRD for the ship-board standard for siderite matches that for Sample 516F-58-2, 46–47 cm reasonably well. This mineral also occurs in several samples from Site 21 (Rex, 1970). An unidentified peak at about $28.3^\circ 2\theta$ in XRDs from samples from Cores 72, 73, 76, and 77 from Hole 516F may indicate the presence of hypersthene, but the Core 72 and 73 samples in question also generated peaks at 14 and $25^\circ 2\theta$. The XRD for Sample 516F-79-5, 36–37 cm resembles figure 7c of Calvert (1974), indicating that the $21.25^\circ 2\theta$ peak in that diffractogram corresponds to tridymite. Sample 516F-81-1, 53–54 cm is probably contaminated with barite, a constituent of *Glomar Challenger* drilling mud. Barite, however, is also reported in two samples from Site 21 (Rex, 1970).

Correlation of Mineralogy with Physical Properties and Seismic Stratigraphy

The correlation between mineralogy and physical properties at Site 516 is excellent. Four levels are corre-

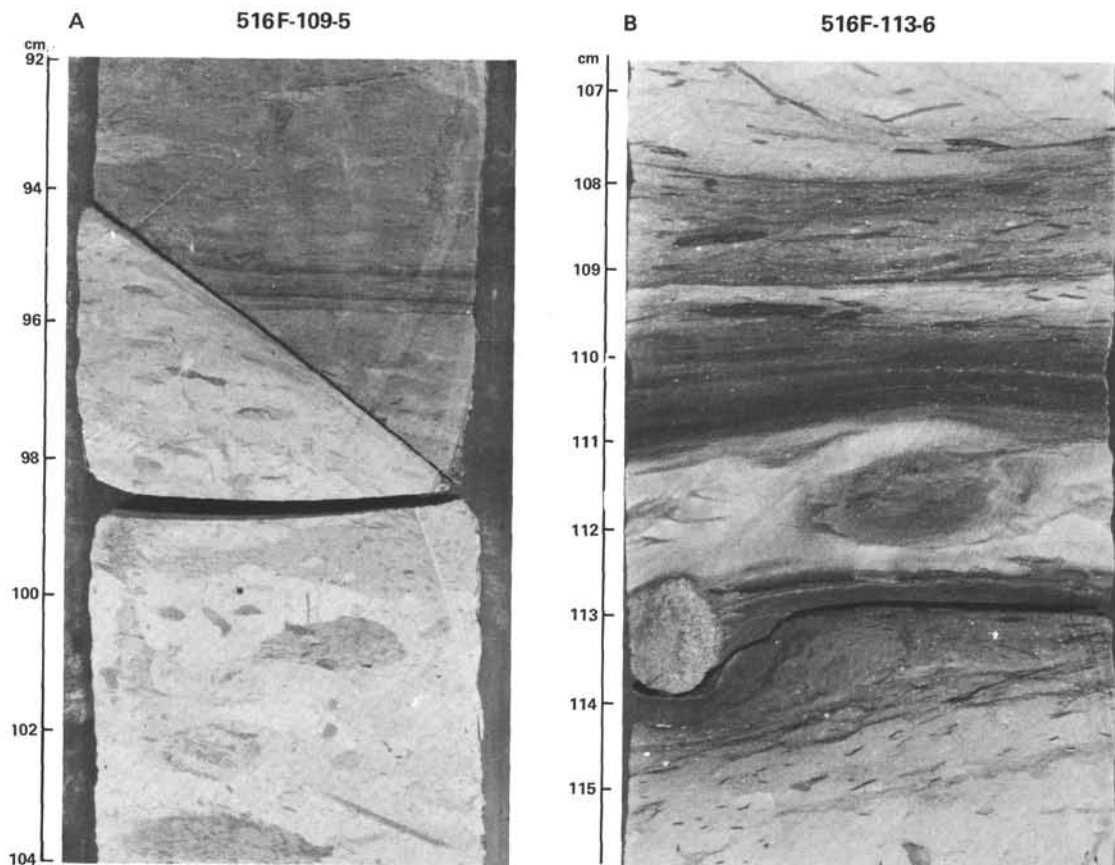


Figure 15. Details of unusual features in Lithologic Subunit 6b, Site 516. A. 516F-109-5, 92–104 cm, offset juxtaposes, contrasting colors. B. 516F-113-6, 106–116 cm.

lated with reflectors seen on seismic profiles across the site (Figs. 25 and 26 of Site 516 chapter, this volume; Barker et al., this volume). The first reflector is placed at 180 m sub-bottom (0.22 s). Although not associated with a mineralogic change, this level closely matches the ooze-chalk transition noted for Core 516F-2 (Site 516 chapter, this volume). A velocity change (not included in the data excerpts shown in Fig. 9) corresponds to a seismic reflector at 330 m sub-bottom depth (0.40 s) and is coincident with the Unit 2/Unit 3 transition and the appearance of illite and montmorillonite. Velocity increases almost linearly with sub-bottom depth until the middle of the middle Eocene. As ash beds become numerous and lithology varied, the scatter of the sonic velocity data increases markedly. Despite the scatter, velocities increase markedly between Cores 47 and 79, paralleling an increase in opal-CT registered in XRDs beginning with Core 58. A “midsection domes” reflector (660–680 m sub-bottom) was thought to represent patch reefs, sills, or volcanic basement, and the total sedimentary section was estimated to be 800 m thick (unpublished cruise prospectus, Leg 72). Shipboard sedimentology and XRD analysis indicate that the “midsection domes” reflector arises from chertified limestones and has a diagenetic rather than a primary depositional origin. Even drilling at Sites 21 and 22 (Maxwell et al., 1970d) had indicated a similar association. As expected, the increase in opal-CT content produces cor-

responding increases in density and decreases in porosity of the sediment in general (Schafenaar et al., this volume). As opal-CT concentrations and occurrences diminish between Cores 79 and 81 in Hole 516F, sonic velocity decreases markedly then rises gradually through Subunits 5b and 6a as dolomite is registered in the diffractograms.

The predictive value of seismic stratigraphy was put to test at Site 516. A last reflector on the *Glomar Challenger* seismic profile was crossed at about the Subunit 6a/6b contact (1125 m sub-bottom, 1.07 s), a level where measured samples show a sudden increase in sonic velocity corresponding to increased quartz concentrations (Fig. 9). No other reflectors remained, and drilling proceeded “seismically blind” for another 127 m of section until basalt was recovered at the base of Core 516F-125; the position of the basalt registered no mark on the seismic profiles.

Comparison of Sedimentation at Rio Grande Rise DSDP Sites 21, 22, 357, and 516

The general pattern of sedimentation at Sites 357 and 516 is quite similar (Fig. 2). Site 357 is located in deeper water than Site 516, on a ridge more distant from the crest of the Rio Grande Rise (Fig. 1). Correlation of these two sites with Sites 21 and 22 is more difficult because of the condensed nature and spot-coring of the earlier drilled sites (Table 1, Fig. 2).

At both Sites 357 and 516, the Oligocene to Recent sections are composed of pelagic limestones, chalks, and oozes. Eocene volcanism is manifest at Site 357 by at least one ash bed and montmorillonite, but the Site 357 chapter (Perch-Nielsen et al., 1977) gives the impression that ash deposits are much rarer at Site 357 than at Site 516, perhaps because of the more distal position of Site 357.

"Cristobalite" occurs as "friable cherty carbonate rock" in the Oligocene sediments of Site 22 (Maxwell et al., 1970c; Rex, 1970), as "chert" in "small brownish gray stringers" in the Eocene of Site 357 (Perch-Nielsen et al., 1977c); also, it replaces foraminifers and occurs as cement, as at Site 516. The widespread occurrence of middle Eocene Atlantic deep-sea cherts was one of the early discoveries of DSDP (e.g., Heath and Moberly, 1971; Ramsay, 1971; Berger and von Rad, 1972). On a broader scale, chert is characteristic of Eocene sediments of the world ocean basins. In a discussion related to the chance recovery of a well-preserved, nonchertified assemblage of middle Eocene planktonic foraminifers, Coulbourn and Resig (1979) summarized examples of chertification, hiatuses, and singularly poor recovery and preservation of similar assemblages in cores from DSDP sites in the Caribbean Sea, and the central Pacific and western Indian oceans (Saunders et al., 1973; Douglas et al., 1973; van Andel and Moore, 1974; Vincent, 1974). Viewed in this perspective, the preservation of the relatively thick Eocene carbonate lithologic section at Sites 357 and 516 is atypical, a direct result of the shallow depths of the Rio Grande Rise. The source of silica for chertification (biogenic and volcanic sources are the prime contenders) is a subject of considerable debate (Wise and Weaver, 1974) and is beyond the scope of this discussion, other than to emphasize the close association of chert and montmorillonite in both the Eocene and Coniacian sediments of Site 516 (Fig. 9).

An allochthonous deposit of Eocene age (Unit 3) occurs at Site 357 (Fig. 2), but spot-coring camouflages the contact of the deposit with the sediments above and below (Perch-Nielsen et al., 1977c). Convolute and dipping beds in Unit 4 at Site 516 qualify portions of that section as 'allochthonous' as well (Fig. 10), detracting from the seemingly exotic nature of Unit 3 of Site 357. There is no counterpart for the Eocene dolostone of Site 357 at Site 516. Dolomite is, however, typical of the Cretaceous deposits at both sites. Because dolomite is poorly represented in the continuously cored Tertiary of Site 516, it is tempting to speculate that its occurrence in Unit 3 of Site 357 is related to a slumped mass of the same nature as, but more distal than, that sampled near the base of Unit 4 of Site 516 (Fig. 9). A pronounced velocity decrease occurs at 443 m sub-bottom at Site 357. As at Site 516, the decrease is near the Eocene/Paleocene boundary and is also associated with a reduction in chert content (figs. 8 and 12 of Perch-Nielsen et al., 1977c).

The flaser bedding so distinctive in the Paleocene and Maestrichtian chalks from Site 516 is apparently not developed in Site 357 cores, where time-equivalent deposits occur under about 400 m less overburden. Only the photograph for Core 357-2 (Perch-Nielsen et al., 1977c)

shows features suggestive of this pressure solution phenomenon. Garrison and Kennedy (1977) mention that flasher structures have been recovered in many DSDP coccolith-rich chalks, but in the two examples they cite, these features are apparent only in the core photographs for Core 216-23 (von der Borch et al., 1974) and Core 223-27 (Whitmarsh et al., 1974). In contrast to the examples from Site 516 (Fig. 13), these features are so vague and sparse that they merited no mention in the description of lithology presented in either site chapter.

Because the Cretaceous/Tertiary boundary was not recovered at Site 357 (it falls within a 9.5-m washed interval between Cores 357-30 and 357-31), no comparison with Core 516F-89 is possible. The boundary was recovered at Site 21, but not as a continuous stratigraphic sequence (Maxwell et al., 1970b). Although there are differences in sample population, the Cretaceous mineralogy of Sites 357 and 516 is quite similar. Illite accounts for a trace or low proportion of the bulk mineral assemblage at Site 516 (Fig. 9) but, with the exception of a few samples, makes up more than half of the carbonate-free clay mineral assemblage at Site 357 (Zimmerman, 1977). Montmorillonite is present in most samples from the Cretaceous of the Rio Grande Rise, and dolomite is present in the Eocene and Cretaceous of Sites 21 (Rex, 1970), 357 (Perch-Nielsen et al., 1977c), and 516 (Fig. 9).

Kaolinite is detected in XRDs of samples of Maestrichtian clays of Site 357 (Zimmerman, 1977), but is either absent or too dilute to be detected in the bulk XRDs of correlative samples from Site 516. In contrast, the pattern for kaolinite distribution in the Campanian rocks is quite similar for both sites (compare Fig. 9 with fig. 5 of Zimmerman, 1977). A detrital deposit derived from tropical weathering (Carroll, 1970), kaolinite may reflect sedimentation from emergent island groups or from continents adjacent to the comparatively small Campanian South Atlantic Basin. This interpretation is supported and refined by the co-occurrence of kaolinite and *Inoceramus* in the Santonian sediments of Site 516. *Inoceramus* remains are restricted to Santonian sediments at Site 357 (Thiede and Dinkelman, 1977), but those Santonian deposits lack kaolinite. *Inoceramus* was found in sediments as young as the Maestrichtian at nearby Site 21 (Maxwell et al., 1970b). A compilation of *Inoceramus* occurrences in sediments from DSDP sites shows their preference for poorly oxygenated, muddy substrate, where they probably lived as epibenthos (Thiede and Dinkelman, 1977). That lithologic association and the scarcity of benthic infauna in the same deposits led Thiede and Dinkelman (1977) to suggest that for these occurrences the interface between anaerobic and aerobic conditions was coincident with the sediment-water interface. Similarly, *Inoceramus* is the only megafossil occurring in the poorly laminated, dark gray sediments of Subunit 6b, Site 516. Ample traces indicate that *Inoceramus* shared this habitat with *Zoophycos*, perhaps a sea pen also capable of straddling the interface between anaerobic and aerobic conditions (Bradley, 1973). As at Site 357, an upper continental slope to outer shelf environment in sediments beneath an oxy-

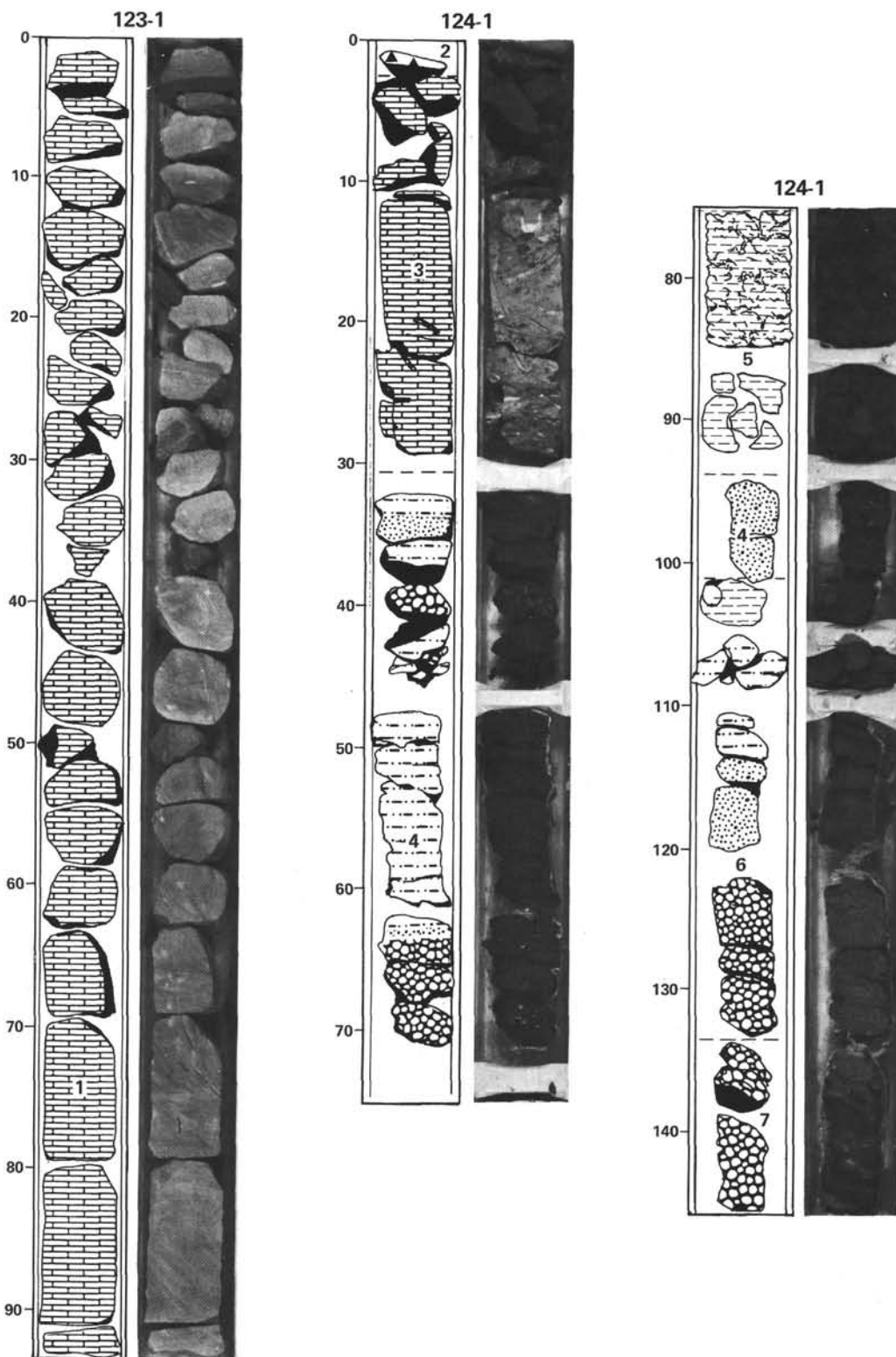


Figure 16. Heterogeneous lithology of Cores 123, 124 and 125 from Hole 516F. Symbols for lithologies as in Figure 2. Dashed lines separate contrasting lithologies identified by numbers. XRDs for these cores are noted within parentheses, according to their sample number listed in Figure 9; color descriptions are followed by their Munsell code equivalents: (1) limestone: white to gray, *Inoceramus*-bearing, Coniacian. (2) ferruginous chert (124-1-9). (3) limestone: pale red (10R 6/4), baked, *Inoceramus*-rich (124-1-16, 124-1-21). (4) mudstone: dusky red (10R 3/2), sandy with thin coarse-grained layers, green (glaucinite?) grains more abundant toward 124-1, 40 cm, matrix gradually becomes green-black (5GY 2/1) and dusky blue-green (5BG 3/2) near 60–70 cm (124-1-67, 124-1-102). (5) montmorillonitic clay: drilling deformed, green clasts in green matrix (124-1-79). (6) montmorillonite-rich graded beds: green-gray (5G 6/1) to blue-green (5BG 3/2) (124-1-136). (7) breccia: green clasts in a grayish red-purple (5RP 4/2) montmorillonitic groundmass, *Inoceramus* common (124-1-138). (8) sandy mudstone: light brown-gray (5YR 6/1) with coarse lithic fragments. (9) sandy montmorillonitic clay: drilling deformed, dusky green altered volcanic ash(?). (10) sandstone: light gray to dusky blue-green (5BG 3/2), graded, numerous green clasts (125-1-90). (11) calcarenite: yellow-gray, bioturbated, recrystallized. (12) basalt.

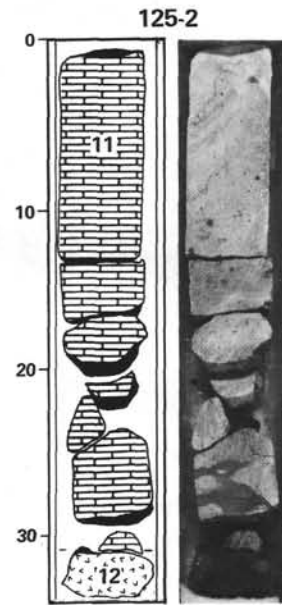
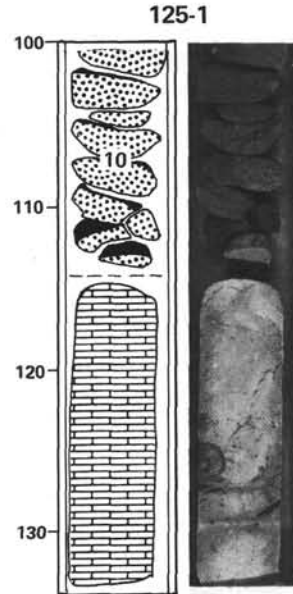
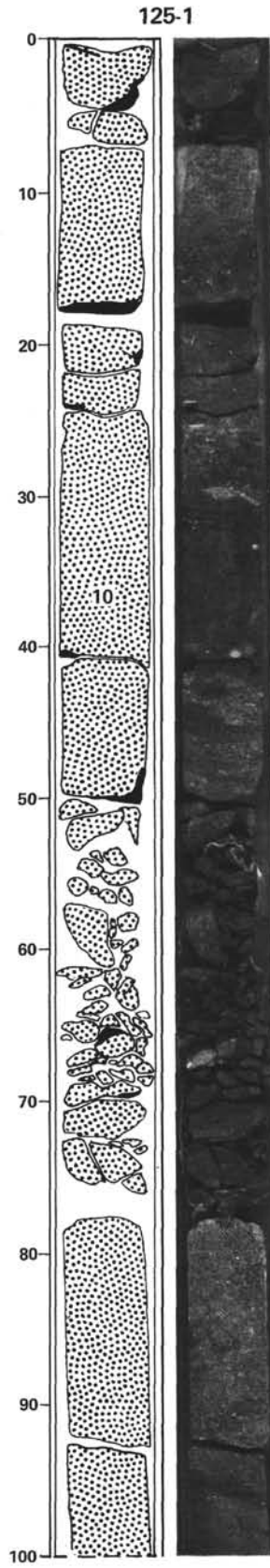
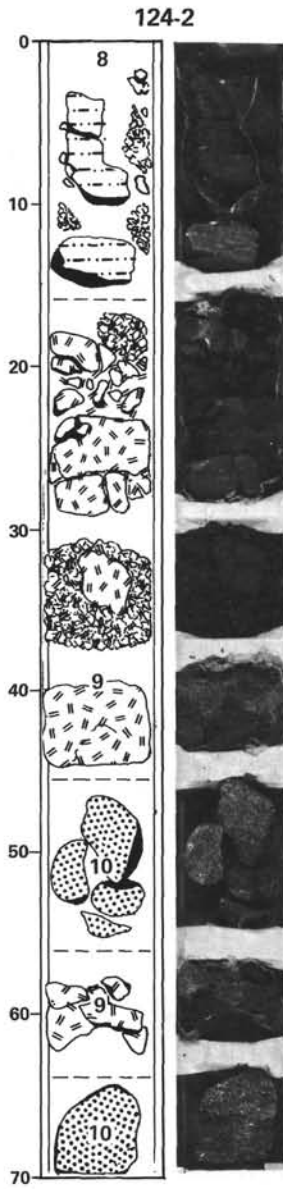


Figure 16. (Continued).

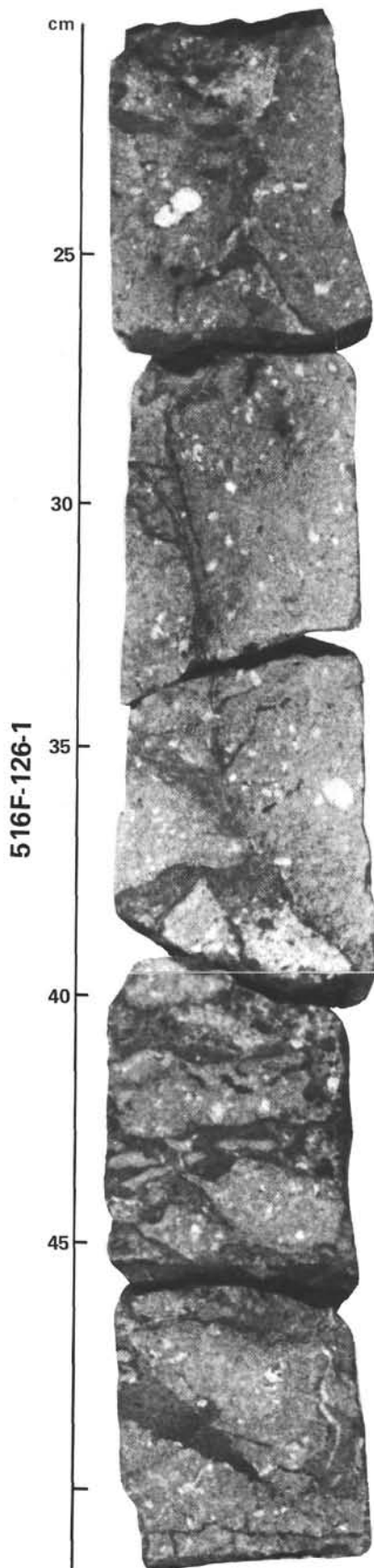


Figure 17. Veined basalt of Section 516F-126-1, representative of large portions of Cores 126 and 127.

gen-minimum zone is the most likely setting for the Santonian deposits at Site 516. In agreement, Barker's (this volume) subsidence curve places the Santonian seafloor at Site 516 near 500 m depth. The presence of kaolinite at Site 516 but not at Site 357 suggests that Site 516 was located downwind of a local subaerial exposures, perhaps islands, from which aerosols or stream discharge could reach Site 516, but not Site 357.

The Leg 3 scientific party described the lowest sample cored at Site 21 as a coquina, a porous well-sorted biosparite (Maxwell et al., 1970b). The green staining, microfossil assemblage, and age of Core 21-9 recall similar attributes of Core 516F-124 (Fig. 16), suggesting that drilling at Site 21 stopped just short of basement.

SITES 517 AND 518, RIO GRANDE RISE NEAR THE VEMA CHANNEL

Background

Sites 517 and 518 were cored by HPC to 50.9 and 76.7 m sub-bottom, respectively (Fig. 2). Their locations, on the flank of the Rio Grande Rise near the Vema Channel, were chosen to complete the DSDP depth transect on the Rio Grande Rise (Table 1, Fig. 1). Given poor weather and only a few days remaining before our required time of arrival in Santos, Brazil, we were fortunate to be able to complete HPC holes at both sites. These two holes extend the record already available in piston core transects (e.g., Ledbetter, 1979).

Results

Twelve HPC cores were taken at Site 517 and all contained a foraminiferal-nannofossil ooze (Site 517 chapter, this volume). The most pronounced features are the coring deformation in the first section of each HPC core (Walton et al., this volume), resulting from vertical motion of the unsupported bottomhole assembly in heavy seas. The sediment is a monotonous, very pale brown. Calcite peaks dominate the nine XRDs from this site and quartz peaks rise just above the background noise level (Fig. 18). Although pteropods were noted in smear slides, no aragonite peaks were registered on the diffractograms. Evidently calcite is so abundant in these sediments that other signals are completely masked.

Calcite dominates all but one of the 30 XRDs made from Site 518 samples. Quartz and illite are of secondary importance and feldspar, montmorillonite and phillipsite occur sporadically. Core 518-15 is calcite poor, the result of intense dissolution during the middle Miocene. This illite-rich interval presumably marks a time of more voluminous northward flow of AABW, a visually recognizable event of the type tracked more precisely by variations in grain-size distributions (Ledbetter, 1979). The event recorded in Core 518-15 is presumably the rise of the upper surface of more calcite-corrosive AABW, replacing LCPW (Barker et al., 1981; Site 518 chapter, this volume).

INTERPRETATIONS

A detailed record of climate fluctuations is held in the microfossil assemblages at Sites 516, 517, and 518 (Ver-

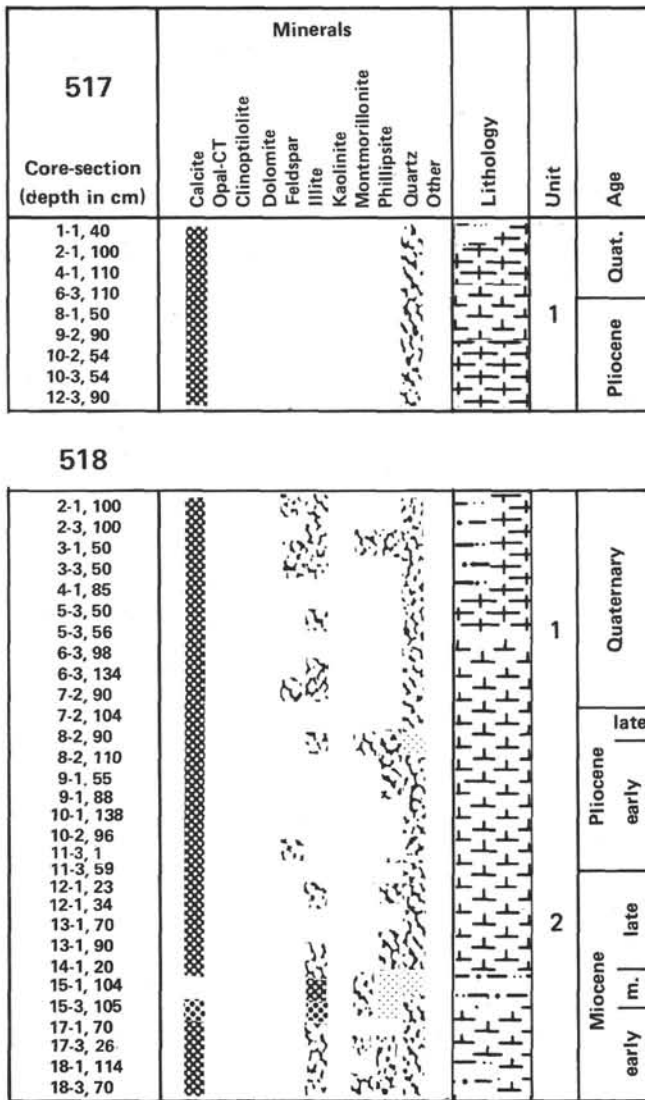


Figure 18. X-ray mineralogy of 39 bulk samples from Sites 517 and 518. Lithology, unit designations, and age assignments are from the site chapters for Sites 517 and 518 (this volume). * indicates replicate analysis. Shading patterns as in Figure 3.

gnaud Grazzini et al., this volume; Pujol and Duprat, this volume; Barash et al., this volume). Site 515, however, contains only sparse calcareous microfossils, and the biogenic siliceous remains accumulated there do not supply the equivalent detail (Johnson, this volume; Gombos, this volume). Nor do XRDs of bulk samples lend themselves to the type of high-resolution paleoclimate reconstructions drawn for places like the eastern Atlantic offshore of northwest Africa (Lange, 1982). The vertical distributions of clay minerals at Site 515, however, do indicate climate transitions in the middle Miocene and between the Oligocene and lower Eocene, but trends within each lithologic unit are vague. The middle Miocene change from illite-rich and kaolinite-rich sediments above to montmorillonite-rich muds below is correlative neither with a similar shift at about 2 Ma in north central Pacific cores (Jacobs and Hays, 1972) nor with the disappearance of illite in Hole 516A and appearance of

montmorillonite in Hole 516F. Calcite is so abundant at Site 516, however, that the clay mineral record is difficult to follow in XRDs from those bulk samples. The pattern of mineral deposition at these sites, however, does correspond to Chamley's (1979) general climate-related scenario for late Eocene to late Pleistocene mineral suites in North Atlantic DSDP sites. Illite, quartz, and feldspar tend to increase as montmorillonite decreases, trends attributed to climate change and increased deep circulation. With progressive cooling, chemical weathering on the continents diminishes in importance and physical erosion of exposed rocks increases. Assuming that the bulk of nonbiogenic sediment accumulated in the deep oceans is detrital, Chamley's (1979) hypothesis invokes a gradual increase of importance of mechanical weathering at the expense of chemical weathering products dominant in older sediments. The abundance patterns for Site 515 (Figs. 3 and 4) and, to a lesser extent, for Site 516 (Figs. 8 and 9) support his assumptions.

Climate-related effects are perhaps documented in the middle Miocene dissolution pulse at Site 518 and in the Eocene-Oligocene unconformity at Site 515; both events were related to intensification of northward AABW flow through the Vema Channel. Clinoptilolite-rich muds at Site 515 may also serve as secondary indicators of climate, because this zeolite might be related to the increased importance of chemical weathering during intervals of relatively warm climates such as the Eocene (Nathan and Flexer, 1977). The increase in silica input during such times would presumably favor the formation of authigenic clinoptilolite. Nathan and Flexer (1977) also suggest that clinoptilolite is an indicator of salinity fluctuations, the lower magnesium content of less saline water favoring clinoptilolite formation. Could clinoptilolite abundance fluctuations serve as an indicator of bottom-water conditions?

Although both transitions in mineral assemblages at Site 515 are correlative with seismic reflectors, and both of those reflectors are attributed to episodes of erosion (Gamboa et al., this volume), only at the lower of the two does the lithologic section hold evidence for erosion. Likewise, most of the seismic reflectors intersected at Site 516 do not correlate with erosional or tectonic events. The patterns of sonic velocity measurements at both Sites 515 and 516 are clearly related to mineral assemblages and patterns of diagenesis on the Rio Grande Rise (Fig. 9) and in the Brazil Basin (Fig. 4).

In contrast to the very general record of paleoclimate available from the lithology and mineralogy of Leg 72 sites, the record of tectonic events and physiography is clear. The occurrence of hydrothermal activity near the mid-ocean ridge is preserved in the veined basalt of Core 516F-126. Algal balls and bryozoans, suspended in the vein-filling matrix, indicate formation of this segment of the Rio Grande Rise at depths within the photic zone (Milliman, this volume). Coniacian volcanism and subsidence are recorded in ash, sands, and graded beds of Cores 516F-124 and 516F-125 (Fig. 12). These coarse-grained deposits and shallow-water microfossils give way upsection to dark, *Inoceramus*-rich Santonian limestones, indicating rapid subsidence to bathyal depths in

a relatively small, semirestricted basin. Decreases in the relative abundance of quartz in the lower Campanian followed by the disappearance of kaolinite in the upper Campanian, parallel color changes from dark gray to alternating green and red tints and finally shades of red-brown in the Maestrichtian. These trends suggest a depositional environment that was becoming more oxidizing through time as the ocean basin at Site 516 widened and distances from terrigenous sources increased. Fluctuating productivity and variable rates of detrital sedimentation, or variable bottom currents, are probably responsible for the pink to red-brown limestone-marly limestone (calcite-illite) alternations characteristic of the Maestrichtian. Fluctuations in calcite preservation are probably not important in this case; estimates place the Late Cretaceous CCD deeper than 3000 m (Berger and von Rad, 1972), and subsidence estimates for Site 516 predict a Maestrichtian depth of about 1000 m (Barker, this volume). Chamley (1979) notes the regional occurrence of Santonian to Maestrichtian illite-rich red calcareous marls containing kaolinite, chlorite, quartz, and feldspar. The Maestrichtian sediments recovered at Site 516 fit this general North Atlantic type; moreover, in general appearance they closely resemble the sediments exposed beneath the Cretaceous/Tertiary boundary at the Bottaccione section near Gubbio (personal observation, and Arthur and Fischer, 1977). Although not necessarily related to strong north-south marine currents as Chamley (1979) has proposed, the wide geographic distribution of this facies does suggest a common element in the opening and circulation within the Atlantic and Tethyan basins.

At the close of the Paleocene this "textbook" model of seafloor spreading and subsidence (Hess, 1962; Sclater et al., 1971) ended, and tectonic rejuvenation occurred (Barker, this volume). Bathymetric gradients and tectonic instability increased to the extent of launching a gravity slide of semiconsolidated Cretaceous limestones from upslope and of interspersing ash and volcanic clasts into the middle Eocene ooze accumulating at Site 516. Patterns of sedimentation remained variable during the middle Eocene; numerous graded beds, sands, and montmorillonite-rich intervals occur throughout. That variability lessened gradually in the late Eocene and Oligocene. The question of whether uplift was sufficient to create a middle Eocene Rio Grande Rise archipelago is perhaps of secondary importance; the larger foraminifers present indicate shelf depths (Tjalsma, this volume), but none of these initial reports for Leg 72 confirms recovery of biogenic remains of subaerial provenance.

As volcanic activity waned on the Rio Grande Rise, northward-flowing AABW was making its way through the Vema Channel. This hypothetical intensified AABW flow was perhaps a result of a "reinforcing teleconnection" between the opening of the Greenland Sea and accelerated NADW production (Johnson, 1982; Tucholke and Miller, 1983). As AABW reached the Brazil Basin, it removed or prevented deposition of at least a portion of the middle and upper Eocene sedimentary record.

NADW flow is credited with production of a correlative erosional feature (Horizon A) over much of the North Atlantic during the same interval of time (Tucholke and Miller, 1983); and equatorial upwelling, enhanced by the flow of Pacific equatorial water across the Isthmus of Panama, was accelerating the rate of accumulation of siliceous skeletal remains (Ramsay, 1971).

If montmorillonite is the echo of the record of volcanism for the region, volcanism did not end with the Eocene, but diminished gradually through the Oligocene at both Sites 515 and 516 (Figs. 4 and 9). Montmorillonite at Site 515 probably does not derive from the same source as at Site 516. At Site 515 it is disseminated and probably derived from a regional source; at Site 516, its source is probably local and it occurs as distinct layers. This contrast is not explained by bioturbation, which is generally more intense at Site 516. Montmorillonite continues into the lower and middle Miocene at Site 515, long after its upper Oligocene disappearance in calcite-rich bulk samples from Site 516, but that difference is probably the result of calcite masking.

The elevation of the Rio Grande Rise presumably created the gradient for ooze-bearing turbidity flows to reach Site 515 (Shor and Rasmussen, this volume), forming calcareous laminations preserved in this deep-water, otherwise clay-rich lithologic section. With the exception of a middle Miocene dissolution pulse at Site 518, normal pelagic sedimentation persisted at all Leg 72 sites, perhaps somewhat too tranquilly at Site 515 for supposed pulsations in AABW flow to influence bedforms or mineral composition.

ACKNOWLEDGMENTS

Richard Myers and Ted 'Gus' Gustafsen made improvements on and maintained the X-ray diffraction unit and peripheral components during the Leg 72 voyage, and Richard assisted in sample preparation and analysis. Victor Sotelo took the core photographs shown in this report. Lola Boyce typed the original and revised versions of this chapter. Peter Barker, Miriam Baltuck, Ralph Moberly, Reinhard Hesse, and Paul Schiffelbein reviewed the manuscript; and Elizabeth Whalen performed a thorough editorial check. I thank each of them for their constructive suggestions.

REFERENCES

- Aoyagi, K., and Kazama, T., 1980. Transformational changes of clay minerals, zeolites and silica minerals during diagenesis. *Sedimentology*, 27:179-188.
- Arthur, M. A., and Fischer, A. G., 1977. Upper Cretaceous-Paleocene magnetic stratigraphy at Gubbio, Italy I. Lithostratigraphy and Sedimentology. *Geol. Soc. Am. Bull.*, 88:367-389.
- Baker, P. A., and Kastner, M., 1981. Constraints on the formation of sedimentary dolomite. *Science*, 213:214-216.
- Barker, P. F., Carlson, R. L., Johnson, D. A., Čepek, P., Coulbourn, W. T., Gamboa, L. A., Hamilton, N., Mello, U., Pujol, C., Shor, A. N., Suzyumov, A. E., Tjalsma, L. R. C., Walton, W. H., and Weiss, H., 1981. Deep Sea Drilling Project Leg 72: southwest Atlantic paleocirculation and Rio Grande Rise tectonics. *Geol. Soc. Am. Bull.*, 92(1):294-309.
- Berger, W. H., 1968. Planktonic foraminifera: selective solution and paleoclimatic interpretation. *Deep-Sea Res.*, 15:31-43.
- Berger, W. H., and von Rad, U., 1972. Cretaceous and Cenozoic sediments from the Atlantic Ocean. In Hayes, D. E., Pimm, A. C., et al., *Init. Repts. DSDP*, 14: Washington (U.S. Govt. Printing Office), 787-954.
- Berger, W. H., and Winterer, E. L., 1974. Plate stratigraphy and the fluctuating carbonate line. In Hsü, K. J., and Jenkyns, H. C.

- (Eds.), *Pelagic Sediments On Land and Under the Sea*: London (Blackwell Scientific Publications), Int. Assoc. Sedimentologists Spec. Publ., 1:11-48.
- Biscaye, P. E., 1965. Mineralogy and sedimentation of Recent deep-sea clay in the Atlantic Ocean and adjacent seas and oceans. *Geol. Soc. Am. Bull.*, 76:803-832.
- Bradley, J., 1973. *Zoophycos* and *Umbellula* (*Pennatulacea*): their synthesis and identity. *Palaeogeogr. Palaeoclimatol. Palaeoecol.*, 13:103-128.
- Briskin, M., and Schreiber, B. C., 1978. Authigenic gypsum in marine sediments. *Mar. Geol.*, 28:37-49.
- Calvert, S. E., 1974. Deposition and diagenesis of silica in marine sediments. In Hsü, K. J., and Jenkyns, H. C. (Eds.), *Pelagic Sediments On Land and Under the Sea*: London (Blackwell Scientific Publications), Int. Assoc. Sedimentologists Spec. Publ., 1:273-299.
- Carroll, D., 1970. *Clay Minerals, A Guide to Their X-ray Identification*: Boulder, CO (Geol. Soc. Am. Spec. Pap. 126).
- Chamley, H., 1979. North Atlantic clay sedimentation and paleoenvironment since the Late Jurassic. In Talwani, M., Hay, W. W., and Ryan, W. B. F. (Eds.), *Deep Drilling Results in the Atlantic Ocean: Continental Margins and Paleoenvironment*: Washington (Am. Geophys. Union), Maurice Ewing Series, 2:342-361.
- Chen, P.-Y., 1977. *Table of Key Lines in X-ray Powder Diffraction Patterns of Minerals in Clays and Associated Rocks*: Bloomington, Indiana (Indiana Geol. Surv.), Occasional Paper 21.
- Cosgrove, M. E., and Papavassiliou, C. Th., 1979. Clinoptilolite in DSDP sediments of the Indian Ocean (Site 223, Leg 23): its stability conditions and estimation of its free energy. *Mar. Geol.*, 33: M77-M84.
- Coulbourn, W. T., and Resig, J. M., 1979. Middle Eocene pelagic microfossils from the Nazca Plate. *Geol. Soc. Am. Bull.*, 90(1): 643-650.
- Douglas, R. G., Roth, P. H., and Moore, T. C., Jr., 1973. Biostratigraphic synthesis: hiatuses and unconformities. In Winterer, E. L., Ewing, J. I., et al., *Init. Repts. DSDP*, 17: Washington (U.S. Govt. Printing Office), 905-909.
- Ellwood, B. B., and Ledbetter, M. T., 1979. Paleocurrent indicators in deep-sea sediment. *Science*, 203:1335-1337.
- Ewing, J., Windisch, C., and Ewing, M., 1970. Correlation of Horizon A with JOIDES borehole results. *J. Geophys. Res.*, 75: 5645-5653.
- Fischer, A. G., and Garrison, R. E., 1967. Carbonate lithification on the seafloor. *J. Geol.*, 75:488-496.
- Garrison, R. E., and Kennedy, W. J., 1977. Origin of solution seams and flaser structure in Upper Cretaceous chalks of southern England. *Sediment. Geol.*, 19:107-137.
- Goldberg, E. D., and Griffin, J. J., 1964. Sedimentation rates and mineralogy in the South Atlantic. *J. Geophys. Res.*, 69:4293-4309.
- Griffin, J. J., Windom, H. L., and Goldberg, E. D., 1968. This distribution of clay minerals in the world ocean. *Deep-Sea Res.*, 15: 433-459.
- Heath, G. R., and Moberly, R., Jr., 1971. Cherts from the western Pacific, Leg 7, Deep Sea Drilling Project. In Winterer, E. L., Riedel, W. R., et al., *Init. Repts. DSDP*, 7, Pt. 2: Washington (U.S. Govt. Printing Office), 991-1007.
- Hess, H. H., 1962. History of the ocean basins. In Engel, A. E. J., James, H. L., and Leonard, B. F. (Eds.), *Petrological Studies: A Volume in Honor of A. F. Buddington*: Boulder, Colorado (Geol. Soc. Am.), pp. 599-620.
- Hsü, K. J., He, Q., McKenzie, J. A., Weissert, H., Perch-Nielsen, K., Oberhansli, H., Kelts, K., LaBrecque, J., Tauxe, L., Krähenbühl, U., Percival, S. F., Wright, R., Karpoff, A. M., Petersen, N., Tucker, P., Poore, R. Z., Gamboa, A. M., Pisciotto, K., Carman, M. F., Jr., and Schreiber, E., 1982. Mass mortality and its continental and evolutionary consequences. *Science*, 216:249-256.
- Jacobs, M. B., and Hays, J. D., 1972. Paleoclimatic events indicated by mineralogical changes in deep-sea sediments. *J. Sediment. Petrol.*, 42:889-898.
- James, H. E., Jr., and Van Houten, F. B., 1979. Miocene goethitic and chamositic oolites, northeastern Colombia. *Sedimentology*, 26:125-133.
- Jenkyns, H., 1974. Origin of red nodular limestones (Ammonitico Rosso, Knollenkalke) in the Mediterranean Jurassic: a diagenetic model. In Hsü, K. J., and Jenkyns, H. C. (Eds.), *Pelagic Sediments On Land and Under the Sea*: London (Blackwell Scientific Publications), Int. Assoc. Sedimentologists Spec. Publ., 1:249-271.
- Johnson, D. A., 1982. Abyssal teleconnections: interactive dynamics of the deep ocean circulation. *Palaeogeogr. Palaeoclimatol. Palaeoecol.*, 38:93-128.
- Kastner, M., 1981. Authigenic silicates in deep-sea sediments: formation and diagenesis. In Emiliani, C. (Ed.), *The Oceanic Lithosphere, The Sea* (Vol. 7): New York (Wiley-Interscience), 915-980.
- Kastner, M., and Stonecipher, S. A., 1978. Zeolites in pelagic sediments of the Atlantic, Pacific, and Indian oceans. In Sand, L. B., and Mumpton, F. A. (Eds.), *Natural Zeolites, Occurrence, Properties, Use*: New York (Pergamon Press), pp. 199-220.
- Lange, H., 1982. Distribution of chlorite and kaolinite in eastern Atlantic sediments off North Africa. *Sedimentology*, 29:427-431.
- Lawrence, J. R., 1979. $^{18}\text{O}/^{16}\text{O}$ of the silicate fraction of recent sediments used as a provenance indicator in the South Atlantic. *Mar. Geol.*, 33:M1-M7.
- Ledbetter, M. T., 1979. Fluctuations of Antarctic Bottom Water velocity in the Vema Channel during the last 160,000 yr. *Mar. Geol.*, 33:71-89.
- Leg 39 Scientific Party, 1975. Leg 39 examines facies changes in South Atlantic. *Geotimes*, 20(3):26-28.
- LePichon, X., Ewing, M., and Truchan, M., 1971. Sediment transport and distribution in the Argentine Basin. 2. Antarctic Bottom Current passage into the Brazil Basin. *Phys. Chem. Earth*, 8: 31-48.
- McCoy, F., Zimmerman, H., and Krinsley, D., 1977. Zeolites in South Atlantic deep-sea sediments. In Supko, P. R., Perch-Nielsen, K., et al., *Init. Repts. DSDP*, 39: Washington (U.S. Govt. Printing Office), 423-443.
- McHargue, T. R., and Price, R. C., 1982. Dolomite from clay in argillaceous or shale-associated marine carbonates. *J. Sediment. Petrol.*, 52:873-886.
- Maxwell, A. E., Von Herzen, R. P., et al., 1970a. *Init. Repts. DSDP*, 3: Washington (U.S. Govt. Printing Office).
- Maxwell, A. E., Von Herzen, R. P., and Shipboard Scientific Party, 1970b. Site 21. In Maxwell, A. E., Von Herzen, R. P., et al., *Init. Repts. DSDP*, 3: Washington (U.S. Govt. Printing Office), 367-411.
- _____, 1970c. Site 22. In Maxwell, A. E., Von Herzen, R. P., et al., *Init. Repts. DSDP*, 3: Washington (U.S. Govt. Printing Office), 413-439.
- _____, 1970d. Summary and conclusions. In Maxwell, A. E., Von Herzen, R. P., et al., *Init. Repts. DSDP*, 3: Washington (U.S. Govt. Printing Office), 441-471.
- Mullins, H. T., Neumann, A. C., Wilber, R. J., and Boardman, M. R., 1980. Nodular carbonate sediment on the Bahamian slopes: Possible precursors to nodular limestones. *J. Sediment. Petrol.*, 50:117-131.
- Nathan, Y., and Flexer, A., 1977. Clinoptilolite, paragenesis and stratigraphy. *Sedimentology*, 24:845-855.
- Newell, R. E., 1974. Changes in poleward energy flux by the atmosphere and ocean as a possible cause for ice ages. *Quat. Res.*, 4: 117-127.
- Officer, C. B., and Drake, C. L., 1983. The Cretaceous-Tertiary transition. *Science*, 219:1383-1390.
- Ogg, J. G., 1981. Sedimentology and Paleomagnetism of Jurassic Pelagic Limestones ("Ammonitico Rosso" Facies) [Unpublished Ph.D. dissert.]. University of California, San Diego.
- Perch-Nielsen, K., Supko, P. R., and Shipboard Scientific Party, 1977a. Site 355: Brazil Basin. In Supko, P. R., Perch-Nielsen, K., et al., *Init. Repts. DSDP*, 39: Washington (U.S. Govt. Printing Office), 101-140.
- _____, 1977b. Site 356: São Paulo Plateau. In Supko, P. R., Perch-Nielsen, K., et al., *Init. Repts. DSDP*, 39: Washington (U.S. Govt. Printing Office), 141-230.
- _____, 1977c. Site 357: Rio Grande Rise. In Supko, P. R., Perch-Nielsen, K., et al., *Init. Repts. DSDP*, 39: Washington (U.S. Govt. Printing Office), 231-329.
- Petzing, J., and Chester, R., 1979. Authigenic marine zeolites and their relationship to global volcanism. *Mar. Geol.*, 29:253-271.
- Prasad, S., and Hesse, R., 1982. Provenance of detrital sediments from the Middle America Trench transect off Guatemala, Deep Sea Drilling Project Leg 67. In Aubouin, J., von Huene, R., et al.,

- Init. Repts. DSDP*, 67: Washington (U.S. Govt. Printing Office), 507-514.
- Rampino, M. R., and Reynolds, R. C., 1983. Clay mineralogy of the Cretaceous/Tertiary boundary clay. *Science*, 219:495-498.
- Ramsay, A. T. S., 1971. Occurrence of biogenic siliceous sediments in the Atlantic Ocean. *Nature*, 233:115-117.
- Reid, J. L., Nowlin, W. D., and Patzert, W. C., 1977. On characteristics and circulation of the southwestern Atlantic Ocean. *J. Phys. Oceanogr.*, 7:72-91.
- Reineck, H.-E., and Singh, I. B., 1975. *Depositional Sedimentary Environments*: New York (Springer-Verlag).
- Rex, R. W., 1970. X-ray mineralogy studies—Leg 3. In Maxwell, A. E., Von Herzen, R. P., et al., *Init. Repts. DSDP*, 3: Washington (U.S. Govt. Printing Office), 509-583.
- Riech, V., and von Rad, U., 1979. Silica diagenesis in the Atlantic Ocean: diagenetic potential and transformations. In Talwani, M., Hay, W. W., and Ryan, W. B. F. (Eds.), *Deep Drilling Results in the Atlantic Ocean: Continental Margins and Paleoenvironment*: Washington (Am. Geophys. Union), pp. 315-340.
- Robertson, A. H. F., 1977. The origin and diagenesis of cherts from Cyprus. *Sedimentology*, 24:11-30.
- Saunders, J. B., Beaudry, F. M., Hay, W. W., Bolli, H. M., Rögl, F., Riedel, W. R., Sanfilippo, A., and Premoli Silva, I., 1973. Paleocene to Recent planktonic microfossil distribution in the marine and land areas of the Caribbean. In Edgar, N. T., Saunders, J. B., et al., *Init. Repts. DSDP*, 15: Washington (U.S. Govt. Printing Office), 769-771.
- Sclater, J. G., Anderson, R. N., and Bell, M. L., 1971. Elevation of ridges and evolution of the central eastern Pacific. *J. Geophys. Res.*, 76:7888-7915.
- Smith, J. V., Beward, A. S., Berry, L. G., Post, P., Weissmann, S., and Cohen, G. E. (Eds.), 1960. *X-ray Powder Data File*: Philadelphia (Am. Soc. for Testing Mins., Spec. Tech. Publ. No. 48-J), index card file.
- Stonecipher, S. A., 1976. Origin, distribution and diagenesis of phillipsite and clinoptilolite in deep-sea sediments. *Chem. Geol.*, 17: 307-318.
- Supko, P. R., Perch-Nielsen, K., et al., 1977. *Init. Repts. DSDP*, 39: Washington (U.S. Govt. Printing Office).
- Thiede, J., and Dinkelmann, M. G., 1977. Occurrence of *Inoceramus* remains in late Mesozoic pelagic and hemipelagic sediments. In Supko, P. R., Perch-Nielsen, K., et al., *Init. Repts. DSDP*, 39: Washington (U.S. Govt. Printing Office), 899-910.
- Tucholke, B. E., and Miller, K. G., 1983. Late Paleogene abyssal circulation in North Atlantic. *Bull. Am. Assoc. Pet. Geol.*, 67:559. (Abstract)
- van Andel, Tj. H., and Moore, T. C., Jr., 1974. Cenozoic calcium carbonate distribution and calcite composition depth in the central equatorial Pacific Ocean. *Geology*, 2:87-92.
- Venkatarathnam, K., and Biscaye, P. E., 1973. Deep-sea zeolites, varieties in space and time in the sediments of the Indian Ocean. *Mar. Geol.*, 15:M11-M17.
- Vincent, E., 1974. Cenozoic planktonic biostratigraphy and paleoecology of the tropical western Indian Ocean. In Fisher, R. L., Bunce, E. T. et al., *Init. Repts. DSDP*, 24: Washington (U.S. Govt. Printing Office), 1111-1149.
- von der Borch, C. C., Sclater, J. G., and Shipboard Scientific Party, 1974. Site 216. In von der Borch, C. C., Sclater, J. G., et al., *Init. Repts. DSDP*, 22: Washington (U.S. Govt. Printing Office), 213-265.
- Wanless, H. R., 1979. Limestone response to stress: pressure solution and dolomitization. *J. Sediment. Petrol.*, 49:437-462.
- Whitmarsh, R. B., Weser, O. E., and Shipboard Scientific Party, 1974. Site 223. In Whitmarsh, R. B., Weser, O. E., Ross, D. A., et al. *Init. Repts. DSDP*, 23: Washington (U.S. Govt. Printing Office), 291-381.
- Wise, S. W., Jr., and Weaver, F. M., 1974. Chertification of oceanic sediments. In Hsü, K. J., and Jenkyns, H. C. (Eds.), *Pelagic Sediments: On Land and Under the Sea*: London (Blackwell Scientific Publications), Int. Assoc. Sedimentologists Spec. Publ., 1:301-326.
- Zimmerman, H. B., 1977. Clay mineral stratigraphy and distribution in the South Atlantic Ocean. In Supko, P. R., Perch-Nielsen, K., et al., *Init. Repts. DSDP*, 39: Washington (U.S. Govt. Printing Office), 395-405.

Date of Initial Receipt: June 1, 1983